A statistical study of the subauroral polarization stream over North American sector using the Millstone Hill incoherent scatter radar 1979–2019 measurements

Ercha Aa[1], Philip J Erickson[2], Shun-Rong Zhang[3], Shasha Zou[4], Anthea J Coster[3], Larisa P. Goncharenko[5], and John C Foster[3]

[1]National Space Science Center, Chinese Academy of Sciences
[2]Massachusetts Institute of Technology
[3]MIT Haystack Observatory
[4]University of Michigan-Ann Arbor
[5]Massachusetts Institute of Technology, Haystack Observatory

November 24, 2022

Abstract

This work conducts a statistical study of the subauroral polarization stream (SAPS) feature in the North American sector using Millstone Hill incoherent scatter radar measurements from 1979 to 2019, which provides a comprehensive SAPS climatology using a significantly larger database of radar observations than was used in seminal earlier works. Key features of SAPS and associated Ne/Ti/Te are investigated using a superposed epoch analysis method. The characteristics of these parameters are investigated with respect to magnetic local time, season, geomagnetic activity, solar activity, and interplanetary magnetic field orientation, respectively. The main results are as follows: (1) Conditions for SAPS are more favorable for dusk than near midnight, for winter compared to summer, for active geomagnetic periods compared to quiet time, for solar minimum compared to solar maximum, and for IMF conditions with negative By and negative Bz. (2) SAPS is usually associated with a midlatitude trough of 15–20\% depletion in the background density. The SAPS-related trough is more pronounced in the postmidnight sector and near the equinoxes. (3) Subauroral ion and electron temperatures exhibit a 3–8\% (50–120 K) enhancement in SAPS regions, which tend to have higher percentage enhancement during geomagnetically active periods and at midnight. Ion temperature enhancements are more favored during low solar activity periods, while the electron temperature enhancement remains almost constant as a function of the solar cycle. (4) The electron thermal content, Te \times Ne, in the SAPS associated region is strongly dependent on 1/Ne, with Te exhibiting a negative correlation with respect to Ne.

A statistical study of the subauroral polarization stream over North American sector using the Millstone Hill incoherent scatter radar 1979–2019 measurements

Ercha Aa[1,2], **Philip J. Erickson**[1], **Shun-Rong Zhang**[1], **Shasha Zou**[3], **Anthea J. Coster**[1], **Larisa P. Goncharenko**[1], **and John C. Foster**[1]

[1]Haystack Observatory, Massachusetts Institute of Technology, Westford, MA, USA.
[2]National Space Science Center, Chinese Academy of Sciences, Beijing, China.
[3]Department of Climate and Space Sciences and Engineering, University of Michigan, Ann Arbor, MI, USA.

Key Points:

- North American SAPS climatology in terms of MLT, season, geomagnetic activity, solar activity, and IMF conditions was comprehensively analyzed
- SAPS is usually associated with a midlatitude trough of 15–20% depletion, which is more pronounced in equinoxes and at midnight
- Both ion and electron temperatures exhibit moderate enhancement around SAPS, with similar geomagnetic but different solar activity dependence

Corresponding author: P. J. Erickson, `pje@mit.edu`

Abstract

This work conducts a statistical study of the subauroral polarization stream (SAPS) feature in the North American sector using Millstone Hill incoherent scatter radar measurements from 1979 to 2019, which provides a comprehensive SAPS climatology using a significantly larger database of radar observations than was used in seminal earlier works. Key features of SAPS and associated $Ne/Ti/Te$ are investigated using a superposed epoch analysis method. The characteristics of these parameters are investigated with respect to magnetic local time, season, geomagnetic activity, solar activity, and interplanetary magnetic field orientation, respectively. The main results are as follows: (1) Conditions for SAPS are more favorable for dusk than near midnight, for winter compared to summer, for active geomagnetic periods compared to quiet time, for solar minimum compared to solar maximum, and for IMF conditions with negative By and negative Bz. (2) SAPS is usually associated with a midlatitude trough of 15–20% depletion in the background density. The SAPS-related trough is more pronounced in the postmidnight sector and near the equinoxes. (3) Subauroral ion and electron temperatures exhibit a 3–8% (50–120 K) enhancement in SAPS regions, which tend to have higher percentage enhancement during geomagnetically active periods and at midnight. Ion temperature enhancements are more favored during low solar activity periods, while the electron temperature enhancement remains almost constant as a function of the solar cycle. (4) The electron thermal content, $Te \times Ne$, in the SAPS associated region is strongly dependent on $1/Ne$, with Te exhibiting a negative correlation with respect to Ne.

1 Introduction

The subauroral polarization stream (SAPS), which was first introduced by Foster and Burke (2002) as a synthesis of previous observational and theoretical work, refers to persistent westward plasma flows driven by enhanced poleward electric fields in the subauroral ionosphere equatorward of the electron auroral precipitation zone. SAPS is predominantly observed in the dusk-midnight magnetic local time (MLT) sector during periods of geomagnetic storms and substorms with a typical width of 3–5°, velocity magnitudes of several hundred m/s or larger, and collocated poleward electric field strengths exceeding 20 mV/m (Foster & Vo, 2002; Erickson et al., 2011). SAPS encompasses a number of occasionally embedded phenomena, including a broader region of smaller drifts (Yeh et al., 1991), as well as latitudinally narrow channels (1–2°) of intense localized westward flow (>1,000 m/s) with stronger electric fields (>100 mV/m), known as polarization jets (Galperin et al., 1974), subauroral ion drifts (SAID) (Anderson et al., 1993, 2001; Spiro et al., 1979), or subauroral electric fields (Karlsson et al., 1998). The presence of SAPS in the coupled ionosphere-magnetosphere plays an important role in controlling the formation and evolution of some large-scale features with significant space weather effects, such as enhanced ion vertical flows (H. Wang & Lühr, 2013), main ionospheric trough (Muldrew, 1965; Spiro et al., 1978; Rodger, 2008), storm-enhanced density plumes (Foster et al., 2007; Zou et al., 2013, 2014), and sunward-convecting plasmaspheric drainage plumes (Goldstein et al., 2004). For these reasons, SAPS/SAID have been extensively studied for several decades using both space-based and ground-based observations. For example, SAID/SAPS signatures can be derived from *in-situ* satellite measurements of ion drifts and electric fields in the ionosphere and/or inner magnetosphere, such as those measured by the Defense Meteorological Satellite Program (DMSP) (e.g., Yeh et al., 1991; Anderson, 2004; Goldstein et al., 2005; Huang & Foster, 2007; H. Wang et al., 2008, 2011; He et al., 2014, 2018; Landry & Anderson, 2018), Van Allen Probes (Foster et al., 2014; Califf et al., 2016; Lejosne & Mozer, 2017), and Magnetospheric Multiscale (MMS) spacecraft (Erickson et al., 2016). Also, the Super Dual Auroral Radar Network (SuperDARN) radars can observe large-scale plasma convection measurements of SAPS continuously over extended periods (e.g., Parkinson et al., 2005; Oksavik et al., 2006; Ebihara et al., 2009; Makarevich et al., 2009; Zou, Lyons, Wang, et al., 2009; Clausen et al., 2012; Nagano et al., 2015; Kunduri et al., 2017, 2018; Z. Wang et al., 2019). Moreover, the altitudi-

nal and time-dependent characteristics (plasma velocities, densities, temperature) on SAPS can also be remotely studied by using powerful incoherent scatter radar techniques (Foster & Burke, 2002; Foster & Vo, 2002; Erickson et al., 2011; Zou, Lyons, Nicolls, et al., 2009).

Various mechanisms have been proposed to interpret SAPS generation, including (1) Voltage source mechanism: During enhanced geomagnetic activity intervals, the inner boundary of the ion plasma sheet penetrates closer to Earth compared to that of electron plasma sheet in the premidnight sector due to their energy spectra difference. This misalignment of the ion and electron boundaries results in a radially outward polarization electric field in the inner magnetosphere (Gussenhoven et al., 1987), which can map along the equipotential magnetic field lines into the subauroral ionosphere in a poleward direction to cause SAPS (De Keyser, 1999). (2) Field-aligned currents (FACs) source mechanism: The ion pressure gradients of the ring current, which is caused by above-mentioned misalignment and/or the pitch angle scattering of precipitation (Yuan et al., 2016), will result in a fraction of downward Region 2 FACs to flow into the duskside subauroral ionosphere, where the conductivity is low due to lacking of electron precipitation (Heinemann et al., 1989). These FACs have to close through poleward Pederson currents with the Region 1 FACs, thus generating strong poleward electric fields (i.e., SAPS electric fields) in the low conductivity subauroral region (Anderson et al., 1993; Raeder et al., 2016). Other studies have also demonstrated that the location of SAPS is conjugate to the peak energy density of the ring current and the Region 2 FACs, and that the magnitude of SAPS velocity is approximately inversely proportional to the flux tube integrated Pedersen conductance (Zheng et al., 2008; H. Wang et al., 2008; He et al., 2014; Yu et al., 2015; Z. Wang et al., 2019). (3) Ionospheric feedback mechanism: The enhanced ion-neutral frictional heating associated with SAPS will accelerate the ion recombination rate, thus reduce the F-region density and create a large upward flow due to thermal expansion (Schunk et al., 1976; Anderson et al., 1991). This process will further reduce the already low subauroral conductivity and provide a feedback effect to amplify the strong electric fields (Anderson et al., 2001). (4) Substorm current wedge mechanism for SAPS and short-circuiting mechanism for SAID. Conventional theories normally involve relatively slow physical processes. However, Mishin et al. (2017) proposed that the broader SAPS and the narrower SAID channels could be separately generated by non-traditional mechanisms, since SAPS/SAID observations show very quick development (∼10 min) shortly after substorm onset. Specifically, downward Region 2 FACs could emerge in response to upward Region 1 FACs via current closure, which results from the arrival of the westward traveling surge of the substorm current wedge. This process builds up a large poleward electric field in the low conductivity subauroral region, which triggers fast ring current injections and SAPS on the dusk side (Mishin, 2016; Mishin et al., 2017). On the other hand, fast SAID response is suggested to be driven by the short-circuiting of the penetration of earthbound substorm hot plasma jets into the plasmasphere (Mishin et al., 2010; Mishin, 2013). Z. Wang et al. (2019) reported a rapid SAPS response to a localized and deep energetic particle injection during non-substorm time and suggested that the plasma pressure increase due to the injection is responsible for the localized SAPS enhancement. Taken in aggregate, these varied theoretical results indicate that more than one mechanism could be responsible for the formation and evolution of SAPS.

Besides observational case analyses, many statistical studies and modeling efforts have been made to characterize SAPS climatology, and its average spatial/temporal variation and activity dependence has been widely studied. Organizing principles of such studies include (1) Local time variation: The average geomagnetic latitude (MLAT) of SAPS tends to locate at the equatorward boundary of auroral precipitation around 60–65° in the dusk and decreases linearly with respect to increasing MLT, reaching 50–55° in the morning. Also, SAPS tends to have largest occurrence rate and peak flow velocity around 20 MLT that decreases toward dawn (Karlsson et al., 1998; Foster & Vo, 2002; Erickson et al., 2011; Kunduri et al., 2017). (2) Geomagnetic dependence: SAPS can be observed both during intense storms with flows exceeding 1,500 m/s and time lags of 0–

1.5 hours after southward turning of the interplanetary magnetic field (IMF), as well as during substorms with flows dropping to 100 m/s and time lags of 0–2.5 hours after IMF southward turning (He et al., 2017; Kunduri et al., 2018). Typically, SAPS tends to move equatorward and has a larger peak velocity with respect to increasing geomagnetic activities (Kp, Dst, AE, and SYM/ASY-H indices) (e.g., Karlsson et al., 1998; Foster & Vo, 2002; H. Wang et al., 2008; Erickson et al., 2011; Kunduri et al., 2017). (3) Seasonal and hemispheric variation: Some studies found that SAPS can be observed more frequently and have larger poleward electric fields during the equinoxes in comparison to solstices (Karlsson et al., 1998; He et al., 2014). However, some other studies indicated that SAPS peak velocities are larger in local winter as compared to summer for both hemispheres (Koustov et al., 2006; H. Wang et al., 2012; H. Wang & Lühr, 2013), and the Pederson currents and the electric fields are generally larger in the winter hemisphere (Kunduri et al., 2012). Furthermore, X. Zhang et al. (2015) indicated that the drift velocities of SAID are generally larger in the Northern Hemisphere than the Southern Hemisphere in all MLT sectors.

Although significant progress has been obtained through these studies, current climatological knowledge of the occurrence and variability of SAPS is still incomplete, and there are some critical issues remaining to be addressed. These include: (1) What is the statistical behavior of electron density and plasma temperature associated with SAPS? Certain features of SAPS (e.g., zonal velocity, electric field, location, conductance) investigated in many prior studies have generally consistent results. Still, some counter-examples exist in particular for ion temperature. For example, some storm-time case studies and numerical simulations have indicated that ion temperature around SAPS region will be greatly enhanced due to frictional heating (e.g., Yeh & Foster, 1990; Anderson et al., 1991; Moffett et al., 1998; Pintér et al., 2006; W. Wang et al., 2012; Erickson et al., 2010; S.-R. Zhang et al., 2017). However, some statistical studies using DMSP measurements indicated that the ion temperature around SAPS peak region shows no apparent enhancement, or could even be depressed (H. Wang & Lühr, 2013; Q. Zhang et al., 2020). Thus, how to interpret these conflicting results and re-evaluate the variability of the plasma temperatures around SAPS region is of considerable interest (2) What is the solar activity dependence of SAPS? The diurnal variation and geomagnetic dependence of SAPS have been widely analyzed as mentioned above. Yet, very few studies have focused on the solar cycle variation of SAPS due to limited coverage of observational databases. He et al. (2014) analyzed DMSP 1987–2012 measurements and found that the narrow SAID channel moves equatorward with larger widths during periods of high solar activities. However, it remains unknown whether the broader SAPS feature has a similar solar cycle dependence, and what the solar activity dependence is of other pivotal parameters (i.e., electron density, ion temperature, electron temperature)? These are essential open questions and need to be further addressed. (3) What is the possible influence of the interplanetary magnetic field (IMF) orientation on SAPS? It is known that the auroral convection pattern is strongly controlled by the magnitude and direction of the IMF (e.g., Heppner & Maynard, 1987; Rich & Hairston, 1994; Weimer, 1995; Ruohoniemi & Greenwald, 1996, 2005). However, there are few results in the literature concerning IMF effects on SAPS morphology and dynamics. For example, He et al. (2017) found that the lifetime of SAPS is linearly correlated with the duration of the southward IMF. Lin et al. (2019) modeled the 2013 St. Patrick's Day storm event and found that SAPS will move equatorward with enhanced velocity and broader width when IMF Bz was becoming more southward. Thus, it is still necessary to conduct a systematic statistical study to verify this possible link further and to specify the relationship between IMF orientation and SAPS evolution.

Previously, Foster and Vo (2002) and Erickson et al. (2011) conducted two significant studies on SAPS by using Millstone Hill incoherent scatter radar data collected in the subauroral ionosphere over two decades. They analyzed the average characteristics of SAPS and summarized the variation pattern of SAPS with respect to MLT and Kp

(Dst). In this study, we extended these important early works to investigate in depth the statistical behavior of SAPS by using Millstone Hill incoherent scatter radar measurements between 1979–2019. The current work provides three major updates over these prior studies: (1) We considerably extended the data coverage to four solar cycles, and provided auroral equatorward boundary measurements alongside the Millstone Hill observations to better distinguish auroral or subauroral flows in constructing reliable SAPS dataset. (2) Besides SAPS itself, we also examined key features of electron density (Ne), ion temperature (Ti), and electron temperature (Te) in ionospheric regions located around SAPS. (3) Besides local time and geomagnetic variations, we further investigated the seasonal, solar cycle, as well as IMF dependencies of SAPS and associated plasma parameters. Results of our study provide partial information on the key questions described above, and provide further information for clarifying the spatial and temporal variation of SAPS. The rest of the paper is organized as follows. Section 2 describes the data and methodology procedure. The statistical results and discussion are given in section 3. The conclusions are presented in section 4.

2 Data and Method

The Millstone Hill incoherent scatter radar has been operated by the Massachusetts Institute of Technology since 1960 and has provided valuable ionospheric measurements with full altitude profiles, including but not limited to plasma convection, electron and ion density, and electron and ion temperature information. The radar system is equipped with a 68-m diameter fixed zenith antenna and a 46 m diameter fully steerable antenna (MISA) with an extensive field-of-view. The MISA antenna was installed at Millstone Hill in 1979 and provides extensive spatial and temporal coverage extending more than 30° in latitude, covering 100–1000 km in altitude, and spanning over 4 hours of local time at F region heights (Foster & Vo, 2002; Erickson et al., 2011). Individual azimuth scans also produce fine-scale plasma measurements with a typical temporal resolution of ∼30 s and an along-beam spatial resolution of ∼100–150 km. Over four decades of MISA availability, long-term observations through both regular yearly program and stormtime alert experiments have built up a large database for auroral, subauroral, and midlatitude ionospheric studies over the North American sector (e.g., Yeh et al., 1991; Buonsanto et al., 1992; Foster et al., 2005; L. P. Goncharenko et al., 2007; S.-R. Zhang & Holt, 2007). Within these observations, SAPS flows readily appear as high-speed westward drifts in the dusk-midnight midlatitude ionosphere equatorward of the auroral oval. In this study, we examined the radar azimuth scan measurements of ion velocity and associated plasma parameters during the years 1979–2019 to construct a SAPS data set and to further analyze SAPS and other related statistical features.

The previous technique for identifying SAPS occurrence was introduced in Foster and Vo (2002) and Erickson et al. (2011). In this study, we further improved this technique and extended the data coverage as follows: (1) Specification of the equatorward auroral boundary: The ion and electron energy flux measurements by precipitating particle spectrometer sensors (SSJ) onboard the DMSP satellites can provide high precision and accurate auroral boundary determination. The DMSP SSJ-4 and SSJ-5 data during 1982-2016 were used by Air Force Research Laboratory to create the Auroral Boundary Index (ABI) data identifying the location of equatorward boundary along the satellite path (Gussenhoven et al., 1981, 1983; Hardy et al., 2008). In this study, for a given azimuth scan of the Millstone Hill incoherent scatter radar, a circular fitting for all available boundary locations within ±60 min was applied to determine an integral boundary distribution under MLT-MLAT coordinates. This choice was guided by many previous studies which report that the shape of nighttime equatorward boundary of the auroral oval can be approximately fitted by a circle (Gussenhoven et al., 1983; Hardy et al., 1989; Kunduri et al., 2017). If there is a data shortage for a given time or the fitting result is not good due to the lack of enough nighttime passes, then an alternative
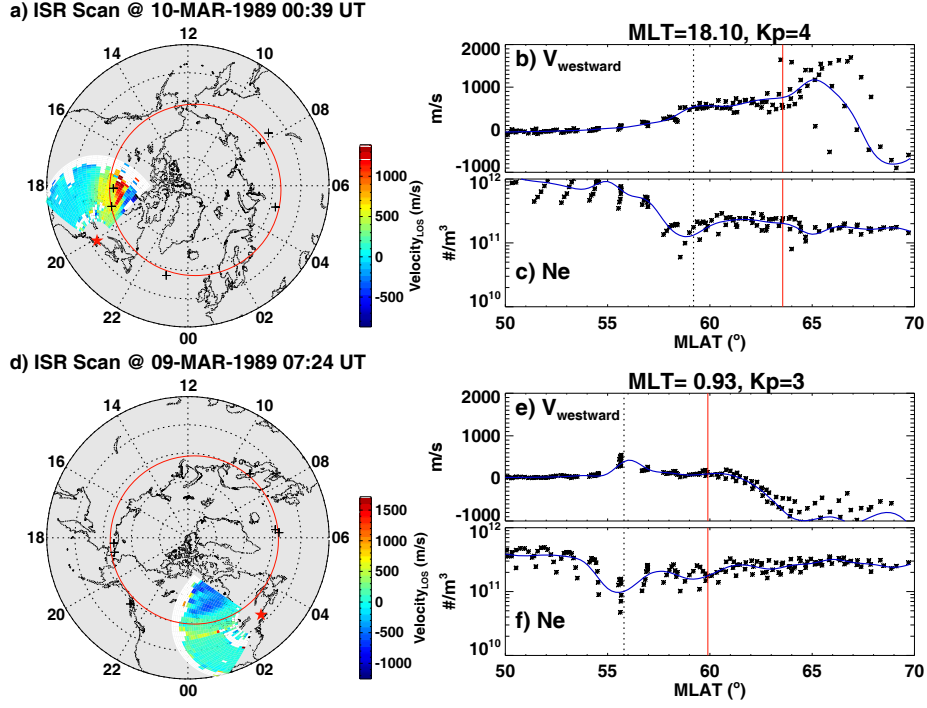
Figure 1. Observations of two SAPS events measured by the Millstone Hill incoherent scatter radar in 9-10 Mar 1989. (a) Line-of-sight plasma velocities for a full azimuth scan in the dusk sector under a polar view of MLT-MLAT coordinate. The concentric dashed circles are plotted in $10°$ interval, with the outermost ring representing $40°$. The red circle represents the fitted equatorward boundary of the auroral oval with the DMSP satellite crossings marked by plus sign (see text for details). (b) Westward velocities and (c) electron densities as a function of geomagnetic latitude, with measurements individually shown by asterisks and collectively fitted by blue line. The red line represents the equatorward auroral boundary and the dotted line marks the identified SAPS peak location. The bottom panels (d–f) are the same as the upper ones, but represent a different azimuth scan near the midnight sector.

Kp-based auroral boundary model was used to implement the boundary determination (Hardy et al., 1987; Carbary, 2005). (2) Computation of the westward component of the flow: The line-of-sight plasma E×B velocity at F region altitudes was measured in each azimuth scan of the radar. Subsequently, the flow measurements were multiplied by a flow-angle correction factor using a cosine of the magnetic direction to calculate the true magnetically westward component. Such a procedure introduces relatively small errors for the predominantly magnetic westward SAPS direction at subauroral altitudes; cf. Erickson et al. (2002). To reduce the errors induced by range discrepancies, we used measurements only in the F region between 300 km and 550 km to extract the SAPS signature. (3) SAPS identification: SAPS was identified as a local peak westward flow that locates below the equatorward auroral boundary, or alternately identified as an inflection point enhancement on the equatorward slope of the convection cell in the dusk sector. The magnitude of SAPS peak velocity was required to be ≥ 100 m/s. On occasion, an associated main ionospheric trough of Ne depletion was used as auxiliary information to help specify SAPS location if the first flow criterion was met. As an example, Figure 1 shows two identified SAPS events in the dusk and midnight sector, respectively. The left panels show the line-of-sight velocities for a full azimuth scan and the fitted auroral equatorward boundary in the MLT-MLAT coordinates. The right panels show the latitudinal variation of the F-region plasma zonal velocities and Ne profiles. SAPS location can be visually identified from the 2D/1D velocity enhancement or inflection point as well as Ne depletion. Following these guidelines, we generated a final data set of more than 1,500 scans containing SAPS out of ∼15,000 separate azimuth scans available from Millstone Hill during 1979–2019.

3 Results and Discussion

Figure 2a shows the temporal coverage and solar cycle variation of the constructed SAPS data set. In general, there were more SAPS events around solar maximum and declining phases than solar minimum. This could be partially due to the fact that geomagnetic activity is often increased during these periods. In particular, coronal mass ejection events occur more frequently in high solar activity years and recurrent geomagnetic activity associated with high speed streams occurs more frequently in the declining phase of solar cycle. However, this yearly variation could also be largely impacted by the availability of original azimuth scan database that is shown in Figure 2c. We note that Millstone Hill experiments are often triggered due to prompt geomagnetic activity indications and thus are not randomly distributed in a synoptic manner with respect to time. Moreover, the measurement composition of different scan modes within each experiment is also highly variable. Only the fraction of Millstone Hill wide coverage azimuth scans with low elevation are appropriate for deriving SAPS. These factors are partially responsible for the uneven distribution of SAPS data set.

Figure 2b and 2d display the seasonal variation of the constructed SAPS data set and original azimuth scan numbers, respectively. The percentage distribution of SAPS occurrence was also given, and error bars were added to evaluate possible biases due to uneven data coverage

$$\sigma = \sqrt{\frac{f \times (1-f)}{N-1}}, \tag{1}$$

where σ is the uncertainty, f is the occurrence rate, and N is the total number of azimuth scans for each given month. The seasonal variation of SAPS occurrence rate is between 5%–15% with two peaks occurring around the equinoxes that are barely affected by the uncertainties. This could possibly relate to the Russell-McPherron effect that equinoctial periods have increased geomagnetic activity with a higher-than-average IMF southward component(Russell & McPherron, 1973). This seasonal pattern is consistent with
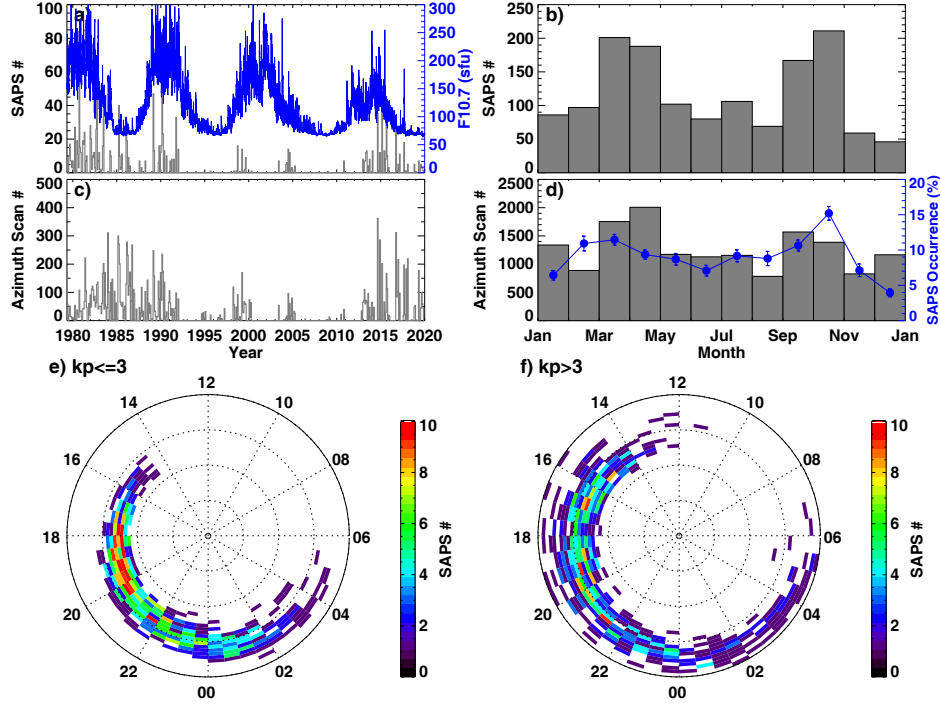
Figure 2. (a and b) Solar cycle and seasonal variation of the constructed SAPS data set. The temporal variation of $F10.7$ index is also plotted. (c and d) Solar cycle and seasonal distribution of the total database of wide coverage azimuth scan for detecting SAPS. The seasonal variation of SAPS occurrence rate is also shown in panel d. (e and f) Distribution of the constructed SAPS data set in the coordinates of magnetic local time and geomagnetic latitude under quiet (Kp≤3) and active (Kp>3) geomagnetic conditions. The concentric circles are plotted in 10° interval with outermost one representing 50° MLAT.

278 previous results (e.g., Karlsson et al., 1998; He et al., 2014), and we will further inves-
279 tigate the seasonal and solar cycle dependence of SAPS in the following subsections.

280   Figures 2e and 2f show the polar distribution of the SAPS data set in the MLT-
281 MLAT coordinates with a resolution of 0.5 hr×1° under quiet and active geomagnetic
282 conditions, respectively. The rightmost column of Table 1 lists the averaged MLAT off-
283 sets equatorward auroral boundary with respect to SAPS peak. Some typical charac-
284 teristics of latitude, local time, and geomagnetic preferences of SAPS can be summarized
285 as: (1) SAPS tends to locate at the equatorward boundary of the auroral precipitation
286 with ∼3–4° offset; (2) SAPS has higher occurrence around dusk time, and its latitudi-
287 nal location gradually decreases with increasing MLT; (3) SAPS peak location is mainly
288 confined within 14–05 MLT during quiet time, with elongation into both earlier and later
289 MLTs as well as equatorward motion with enhanced geomagnetic activity.

290   To proceed with statistical studies, we performed a superposed epoch analysis (SEA)
291 that is similar to those described in H. Wang et al. (2011) and H. Wang and Lühr (2013).
292 The MLAT of SAPS peak velocity was taken as the central point, around which the lat-
293 itudinal profiles of different plasma parameters (velocity, Ne, Ti, Te) were stacked. The
294 average profiles were subsequently calculated, ranging from -10° to 10° off the SAPS peak
295 with a resolution of 0.5°. This method has the goal of investigating the relationship be-
296 tween these parameters as well as their variation patterns with respect to MLT, season,
297 geomagnetic activity, solar activity, and IMF orientation, respectively. Results are de-
298 scribed in following subsections.

3.1 Magnetic Local Time Variation

300   Figures 3a and 3b show the averaged ΔMLAT distribution of zonal plasma veloc-
301 ity derived from the superposed epoch analysis for different MLTs in 2-D and 1-D for-

Table 1.   SAPS peak amplitude and associated plasma parameters for different MLTs, seasons, geomagnetic activity, solar activity, and IMF configurations. The ΔMLAT locations of equatoral auroral boundary (EAB) are shown in the rightmost column.

| | Velocity (m/s) | Ne (10^{11}/m^3) | | Ti (K) | | Te (K) | | EAB |
	Peak	Peak	ΔNe	Peak	ΔTi	Peak	ΔTe	ΔMLAT
Dusk	-728.3	3.28	-16.4%	1595	4.9% (75)	2143	1.9% (42)	3.1°
Midnight	-373.5	2.82	-20.7%	1478	8.0% (110)	1780	5.2% (85)	2.8°
Dec Sol.	-549.1	1.79	-9.1%	1490	5.1% (72)	1976	6.1% (114)	3.3°
Equinox	-576.4	1.65	-20.9%	1603	6.1% (92)	2020	3.3% (65)	3.0°
Jun Sol.	-512.5	1.73	-13.2%	1518	4.2% (62)	2322	2.7% (61)	3.9°
kp≤3	-444.9	1.84	-14.1%	1472	3.7% (53)	1875	1.6% (30)	3.5°
kp>3	-672.4	1.56	-18.9%	1649	7.1% (109)	2220	3.4% (73)	2.9°
$F_{10.7}$≤150	-630.1	1.20	-16.5%	1541	8.5% (120)	2038	2.4% (48)	3.2°
$F_{10.7}$>150	-513.1	2.04	15.7%	1564	4.1% (62)	2014	2.7% (53)	3.4°
+By, +Bz	-554.6	1.70	-13.0%	1462	3.3% (47)	2057	2.3% (46)	3.1°
+By, −Bz	-618.8	1.72	-14.9%	1501	5.5% (78)	2116	4.0% (81)	3.0°
−By, +Bz	-575.7	2.03	-15.2%	1488	2.9% (42)	1797	2.3% (40)	3.2°
−By, −Bz	-716.1	2.12	-15.8%	1545	2.0% (30)	2041	2.0% (40)	3.0°

mats, respectively. The specific values of SAPS-related plasma parameters are listed in Table 1. In general, SAPS peak flows during different MLTs occur around central MLAT of 0 as expected. However, there is a large difference between SAPS features in the dusk (17–21 MLT) and midnight (22-02 MLT) sectors: the dusk-time SAPS channel has a higher peak velocity (-728.3 m/s) and a broader latitudinal width ($\geq 5°$), with the averaged MLAT offsets of the equatorward auroral boundary being $3.1°$. On the other hand, the midnight SAPS channel is more tightly clustered with considerable reduction in width by a factor of two, and the averaged MLAT offsets of the equatorward auroral boundary, determined separately from DMSP observations, is $2.8°$. The midnight SAPS peak velocity (-373.5 m/s) is barely half of the dusk amplitude, and is approximately equal to the average eastward corotation velocity at subauroral latitudes. These results suggest that dusktime SAPS flow could overwhelm the cororation effect and transport ionospheric plasma both sunward and poleward to earlier MLTs, contributing to the formation of storm-enhanced density plumes (Foster, 1993; Kelley et al., 2004), also known as the dusk effect (Mendillo, 2006). On the other hand, nighttime SAPS tends to counteract the corotation flow, and keeps plasma at a constant location in the inertial Sun-Earth reference frame (constant MLT). This dusk-midnight difference of SAPS magnitude and width is consistent with previous studies (Foster & Vo, 2002; Anderson, 2004; Erickson et al., 2011; Kunduri et al., 2017).

Figure 3c and Figure 3d show the ΔMLAT-MLT distribution of electron density associated with SAPS in 2-D and 1-D formats, respectively. Figure 3e shows the relative deviation of electron density with respect to its background values, obtained through a eleven-point ($\sim 5°$) smoothing average. It is known that the enhanced ion-neutral frictional heating associated with SAPS will accelerate nonlinear ion loss processes and thus facilitate formation of the midlatitude trough (Schunk et al., 1976; Rodger, 2008). However, we note in particular that the deepest trough occurs in the postmidnight sector around 00–02 MLT as can be seen from Figure 3c. The line plots in Figure 3e and Table 1 also show that the midnight trough has more severe depletion (-20.7%) compared with that of the dusktime trough (-16.4%). Previous results in the literature are contradictory about the local time when the deepest trough are observed. For example, Tulunay and Sayers (1971) reported that the deepest trough at the height of 550 km occurs near midnight by using Ariel 3 satellite data. Prölss (2007) reported that the largest electron density drops at the height of 350 km were observed around 18 MLT by using Dynamics Explorer 2 data, though this study only analyzed the trough events during 15–21 MLT. In addition, Karpachev (2003) found that the northern hemisphere trough during winter non-storm time (Kp$\leq$3) in the 30-60°W longitudinal sector is slightly deeper in 18-19 LT than 23-01 LT by using Cosmos satellite data at 500 km. These conflicting results may be due to different spatial/temporal coverage and different criteria in identifying troughs, and more future work is needed to address this problem further.

In results here, we report that the SAPS-related midlatitude trough at 300-550 km altitude has more pronounced depletion in the postmidnight sector. Although based on a specific subset of midlatitude trough events, this phenomenon is in agreement with that indicated in Aa et al. (2020) in that the midlatitude trough in the Northern Hemisphere usually exhibits a higher occurrence rate in the postmidnight sector than that of the evening sector. One possible explanation for this result is that the midnight plasma flow around SAPS region is significantly lower than that of dusktime, providing sufficient time for recombination to produce a deeper depletion (Voiculescu & Nygrén, 2007). Around this local time, a convection flow configuration, referred to as the Harang reversal, is often observed, which is a result of the overlap between the Region-2 upward and downward FACs (e.g., Zou, Lyons, Wang, et al., 2009; Zou, Lyons, Nicolls, et al., 2009; Gkioulidou et al., 2009). The high-latitude return flows bifurcate at 01-02 MLT and thus the flow stagnation point between the high-latitude convection and corotation extends to this local time as well.
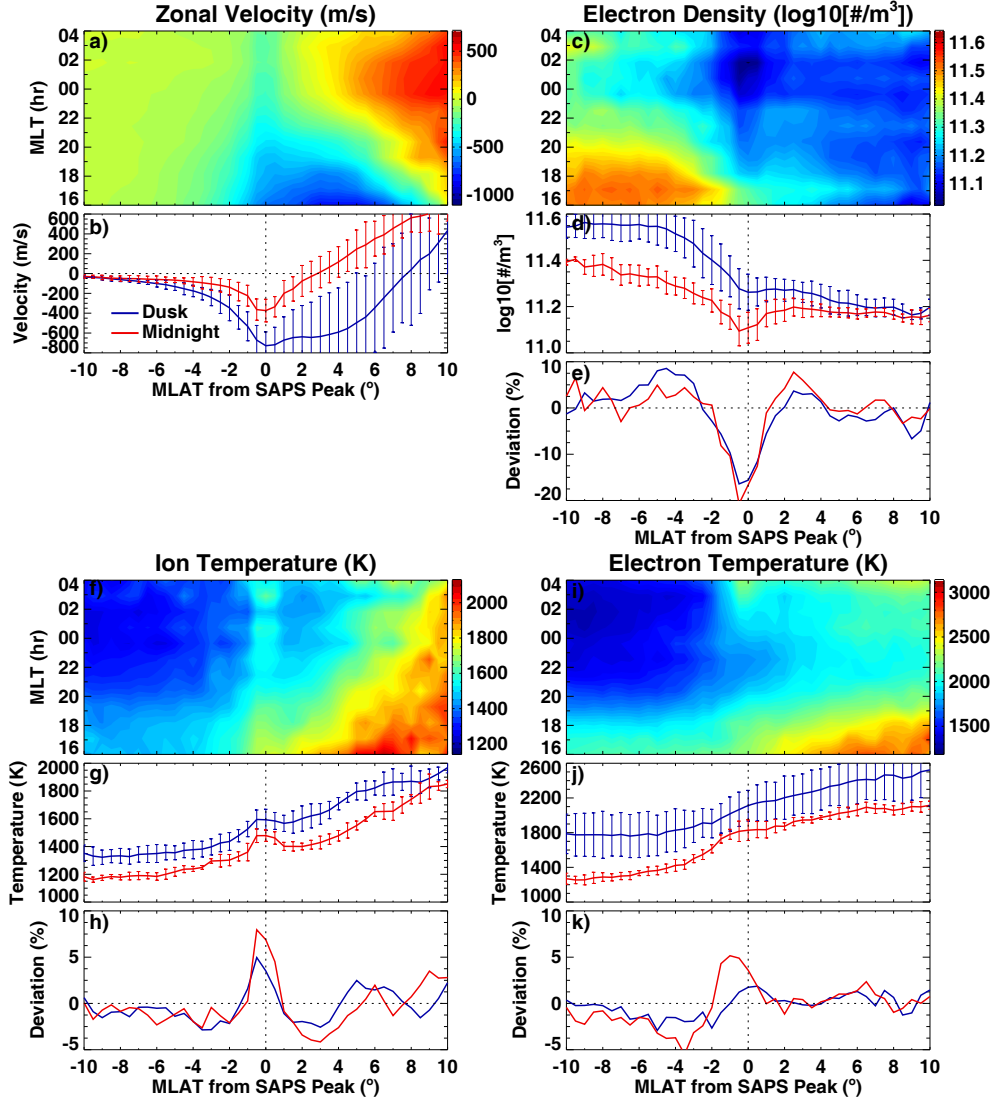
Figure 3. Local time variation of the superposed epoch analysis of SAPS related plasma parameters: zonal plasma velocity (a and b), electron density (c–e), ion temperature (f–h), and electron temperature (i–k), respectively. The key MLAT of "0" represents the location of SAPS peak velocity. The top and middle panels of each group are the 2-D and 1-D distribution. The bottom panels of each group show the percentile deviation of Ne, Ti, and Te with respect to background values, respectively. The blue lines represent the variation patterns around the dusk (17–21 MLT), and the red lines represent those around the midnight (22–02 MLT). The exact amplitudes are recorded in Table 1.

Figures 3f–3h and Figures 3i–3k show the MLT variation of ion temperature and electron temperature associated with SAPS, respectively. Both the ion and electron temperatures exhibit moderate enhancement around SAPS region compared to the background trend. This is consistent with observations from the Dynamics Explorer-2 satellite which show that ion and electron temperature within SAPS-related troughs will be strongly elevated (Moffett et al., 1998). The temperature increment is larger in the midnight sector (Ti: 8.0% (∼110 K) and Te: 5.2% (∼85 K)) than that in the dusk sector (Ti: 4.9% (∼75 K) and Te: 1.9% (∼42 K)). The temperature enhancement are inversely proportional to the electron density decrease within the trough. However, there might be a large altitudinal gradient of the ion temperature since H. Wang and Lühr (2013) reported that the ion temperature around SAPS region at 800 km was reduced ∼30%. Heelis et al. (1993) found that frictional heating can quickly increase the ion temperature to a constant level over a broad altitudinal region between 300 km and 500 km, which is approximately consistent with the current range of Millstone Hill radar measurements. This result also indicates that a new thermal equilibrium between ions and neutrals can be effectively attained. At higher altitudes above 600 km, however, it takes much longer time to increase the ion temperature to a new equilibrium since ion-neutral collisions are much smaller and not as effective at thermal transfer as at lower altitudes. Furthermore, enhanced ion temperature and frictional heating at lower altitudes will result in a large vertical pressure gradient and cause thermal expansion and plasma upward flow. Thus, compared with lower altitudes, frictional heating is less efficient in the topside ionosphere. For these reasons, H. Wang and Lühr (2013) proposed a mechanism in which ion temperature at 800 km is more likely to initially respond to adiabatic cooling associated with plasma expansion from lower altitudes. However, as time progresses, it is expected that thermal conduction and local frictional heating would eventually increase the topside ion temperature in this scenario. Future work is still needed to further study SAPS-related ion temperature variation in the topside ionosphere.

In general, electron temperature in the ionosphere is also determined by the thermal balance between heating and cooling processes. Besides daytime photoelectron heating by solar extreme ultraviolet radiation, it is known that the downward energy and heat transfer from the ring current along magnetic field lines during geomagnetically disturbed periods will cause a subauroral electron temperature enhancement, which usually occurs in association with the midlatitude trough in the nighttime topside ionosphere (e.g., Evans, 1970; Kozyra et al., 1986; Watanabe et al., 1989; Fok, Kozyra, Warren, & Brace, 1991; Afonin et al., 1997; Prölss, 2006; W. Wang et al., 2006). Furthermore, Coulomb collisions with ions provide an important energy loss mechanism for topside ionospheric electrons (Schunk & Nagy, 2000). In the SAPS region, characterized by intense heating and ion upwelling during storm time, energy exchange between the electrons and ions forms the primary cooling processes for thermal electrons in the $F2$ layer. Lower electron density will therefore tend to result in higher electron temperatures because of the greater thermal energy available per particle, and the cooling process will be less efficient due to reduced Coulomb coupling with ions (Schunk & Nagy, 1978; Moffett & Quegan, 1983). Taken in aggregate, the relative enhancement of electron temperature in the SAPS region will therefore be more pronounced around midnight due to more profound trough depletion than that occurring in dusk sectors. This Te-Ne correlation associated with SAPS will be further addressed later.

3.2 Seasonal Variation

Figures 4a–4b and 4c–4e display the averaged ΔMLAT distribution of SAPS-related plasma velocity and electron density for different seasons in 2-D and 1-D formats, respectively. There is a slight winter-summer asymmetry in that the SAPS peak velocity has larger values in winter than summer, with the exact values being recorded in Table 1. Many studies have found that the SAPS velocity is inversely proportional to the flux-tube integrated Pedersen conductivity in the subauroral region, which is primarily con-
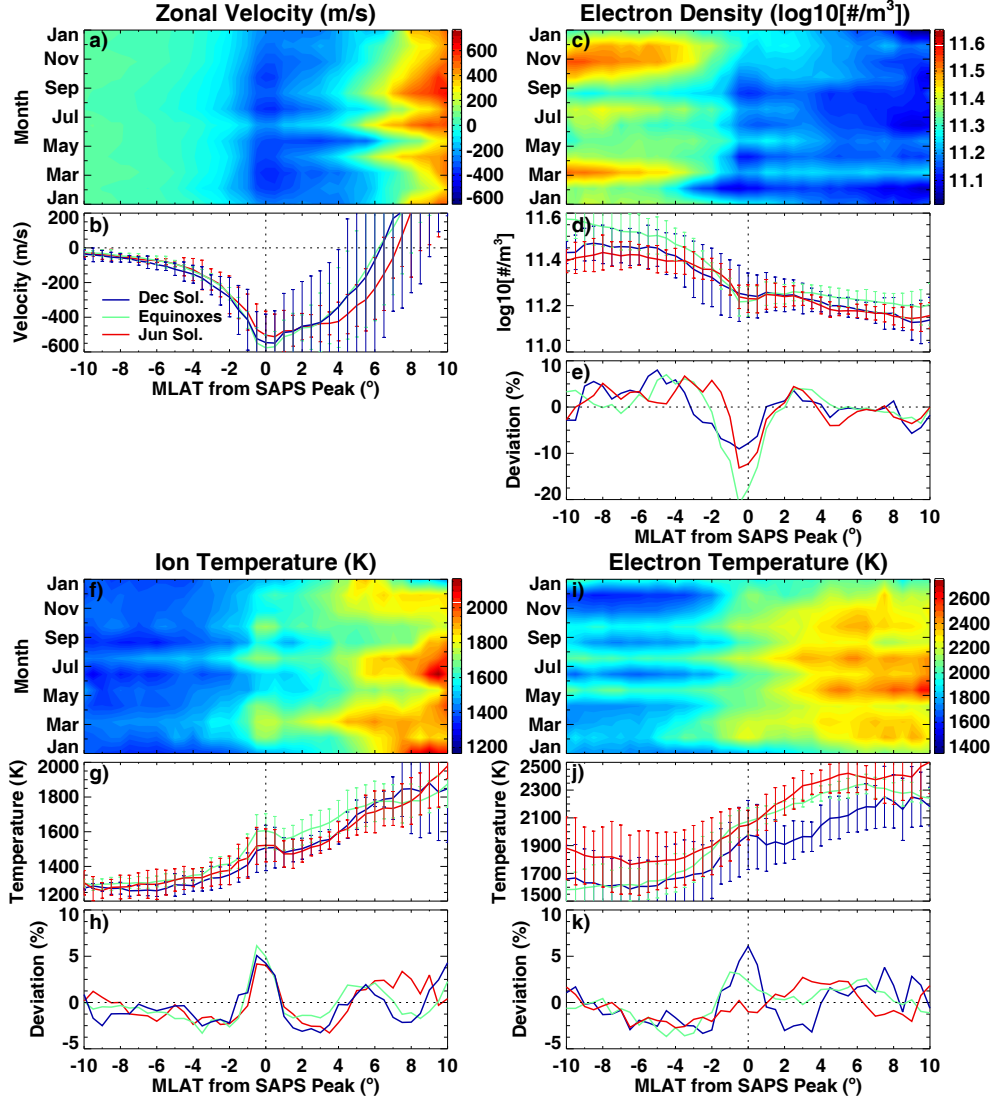
Figure 4. The same as Figure 3, but for seasonal variation. The blue, green, and red lines represent the variation pattern around December solstice (November, December, January, and February), equinoxes (March, April, September, and October), and June solstices (May, June, July, and August), respectively.

trolled by solar illumination (e.g., Zheng et al., 2008; He et al., 2014; Yu et al., 2015). Thus, the smaller conductivity in winter due to insufficient illumination will lead to an enhanced SAPS electric field and flow velocity to maintain the subaurural current continuity. This seasonal asymmetry is also reported in previous studies (e.g., Koustov et al., 2006; H. Wang et al., 2012; H. Wang & Lühr, 2013). However, it is worth noting that this seasonal difference is within uncertainty levels for this study, and it could also be affected by uneven data distribution and variation of solar flux. Future simulation work is still needed to further specify this issue.

The SAPS peak velocity is slightly larger around equinoctial months than local winter, though the difference is quite small ($\sim$30 m/s). The SAPS-related midlatitude trough also exhibits relatively larger depletion around equinoxes (-20.9%) than December solstice (-9.1%). Karlsson et al. (1998) found that the strength of the subauroral electric field has maximum values close to the equinoxes and minimum values around the summer solstice. He et al. (2014) also found that SAID events can be more frequently observed during equinoxes than solstices. This feature may be related to enhanced geomagnetic activity and ionospheric convection flow around equinoxes. In particular, equinoctial periods have increased solar wind driving conditions with a higher-than-average IMF southward component (Russell & McPherron, 1973), and field-aligned ionospheric conductivity is relatively low when the nightside auroral zones of both hemispheres are simultaneously in the darkness around equinoxes (Lyatsky et al., 2001). Both effects will result in an enhanced SAPS velocity with more substantial frictional heating and deeper trough structure. This phenomenon is also consistent with that indicated in Aa et al. (2020), in that the nighttime midlatitude trough has a higher occurrence rate around equinoxes than local winter.

Figures 4f–4h and 4i–4k show the averaged ΔMLAT distribution of SAPS-related ion and electron temperature for different seasons, respectively. For ion temperature, the relative deviation ($\sim$4–6%) is almost seasonally independent. For electron temperature, on the other hand, the SAPS-related enhancement in the December solstice is 6.1% (114 K), while the temperature enhancement during equinoxes is 3.3% (65 K) and is almost negligible in the June solstice. As the background temperature during June solstice is higher than other seasons, relative increase in temperature for the same amount of energy input will likely to be lower. Our results are contextually consistent with previous studies. Evans (1973) found that the seasonal variation of the heat flux flow into the ionosphere from the plasmasphere can reach an order of magnitude, and the lowest heat fluxes occur in summer and highest fluxes in winter. Similarly, Fok, Kozyra, Warren, and Brace (1991) quantitatively confirmed that the downward electron heat flux from the plasmasphere in winter is comparable to magnetospheric heat flux and is larger than during other seasons. Besides heating sources from the magnetosphere, Richards and Torr (1986) indicated that there is a strong inter-hemispheric thermal coupling between conjugate ionospheres at midlatitude, and solar illumination in the sunlit summer hemisphere can make a considerable contribution to heat the conjugate winter hemisphere immediately. All of the mechanisms above can result in a larger increase of electron temperature in winter than in the absence of a sunlit conjugate region.

3.3 Geomagnetic Activity Dependence

Figures 5a–5b and 5c–5e display the averaged ΔMLAT variation of SAPS-related plasma velocity and electron density for different geomagnetic activity levels, respectively. Many previous studies have indicated that both SAPS velocity and associated ion vertical flow velocity will increase with respect to increasing geomagnetic activity (e.g., Foster & Vo, 2002; Erickson et al., 2011; H. Wang & Lühr, 2013; Kunduri et al., 2017), and the midlatitude trough becomes deeper with increasing geomagnetic activity (e.g., Collis & Haggstrom, 1988; Karpachev et al., 1996; Werner & Prölss, 1997; Prölss, 2007; Aa et al., 2020). In the current study, the blue lines represent the quiet time variation pat-
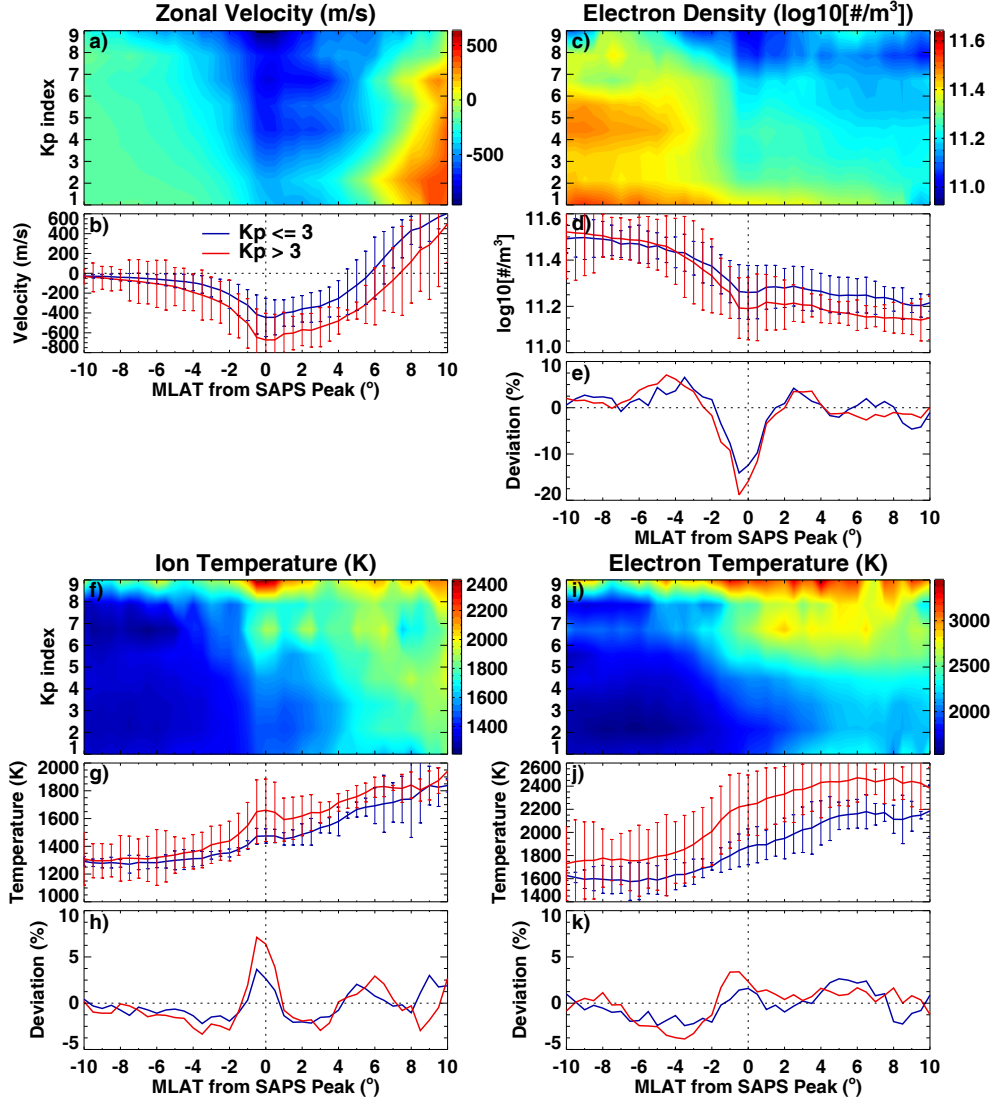
Figure 5. The same as Figure 3, but for different geomagnetic activities. The blue lines represent the variation pattern for Kp≤3, while the red lines represent those for Kp>3.

tern with Kp≤3, while the red lines represent disturbed geomagnetic conditions with Kp>3. It can be seen from both Figure 4 and Table 1 that the disturbed conditions are associated with higher SAPS peak velocity (-672.4 m/s) and deeper trough depletion (-18.9%) than quiet time conditions (-444.9 m/s and -14.1%), respectively. This again confirmed that the increased frictional heating and expansion within the stormtime SAPS region would accelerate the recombination rate and the trough formation.

Figures 5f–5h and 5i–5k show the averaged ΔMLAT distribution of SAPS-related ion and electron temperatures for different geomagnetic activity levels, respectively. Both the ion and electron temperatures exhibit larger enhancement around SAPS region during disturbed geomagnetic conditions that are almost two times of temperature enhancements during quiet conditions. This feature is consistent with that indicated in previous studies (Kozyra et al., 1986; Fok, Kozyra, Warren, & Brace, 1991; Moffett et al., 1998; Prölss, 2006).

3.4 Solar Activity Dependence

Figures 6a–6b and Figures 6c–6e show the averaged ΔMLAT variation of SAPS-related plasma velocity and electron density for different solar activity levels, respectively. The blue lines represent the variation pattern during low solar activity periods ($F10.7\leq150$), while the red lines represent those during high solar activity periods ($F10.7>150$). It can be seen that SAPS has a larger peak value (-630.1 m/s) around low solar activity periods than that around high solar activity periods (-513.1 m/s). This negative correlation between SAPS flow and solar activity is reasonable, as Robinson and Vondrak (1984) and Hardy et al. (1987) indicated that the contribution to the height-integrated ionospheric Pedersen conductivity from solar radiation approximately equals to $0.88\sqrt{F_{10.7}cos\chi}$, where χ is the solar zenith angle. Thus, the weaker Pedersen conductivity around solar minimum will naturally lead to an increased SAPS electric field and flow velocity, as well as an enhanced ion vertical flow. In addition, the co-rotating interaction region during the declining phase of a solar cycle could induce persistent geomagnetic perturbations. This makes the low solar activity years constitute a large number of SAPS events with medium to high level Kp values, which also helps to maintain the SAPS magnitude at a high level statistically.

Moreover, He et al. (2014) indicated that the narrow SAID channel moves equatorward during high solar activity periods. This is in agreement with that mentioned in Le et al. (2017) and Karpachev (2019) that the position of midlatitude trough will move slightly equatorward from low solar activity to high solar activity periods. In our results, the SAPS-related midlatitude trough exhibits almost identical percentile depletion among low and high solar activity periods. Figure 6e shows that the background electron density in high solar activity periods is nearly two times of that in low solar activity, because the enhanced solar extreme ultraviolet radiation associated with higher $F10.7$ will increase the ionization production rate. Thus, it can be deduced that the trough depth, which equals to the product of background density times percentile deviation, should be more significant in high solar activity periods. This is consistent with that mentioned in Aa et al. (2020).

Figures 6f–6h and 6i–6k show the averaged ΔMLAT variation of SAPS-related ion and electron temperature for different solar activity levels, respectively. For ion temperature, low solar activity results exhibit larger enhancement associated with SAPS compared with those during high solar activity periods, which is similar to the plasma flow results. It is important to note that frictional heating depends on both ion-neutral velocity difference and ion density, and therefore the detailed solar cycle variation of SAPS-related Ti and its inter-relationship with frictional heating and electron density might be complicated and involve both ionospheric and thermospheric conditions. Specific simulations are needed to further address this issue in the future. For electron temperature,
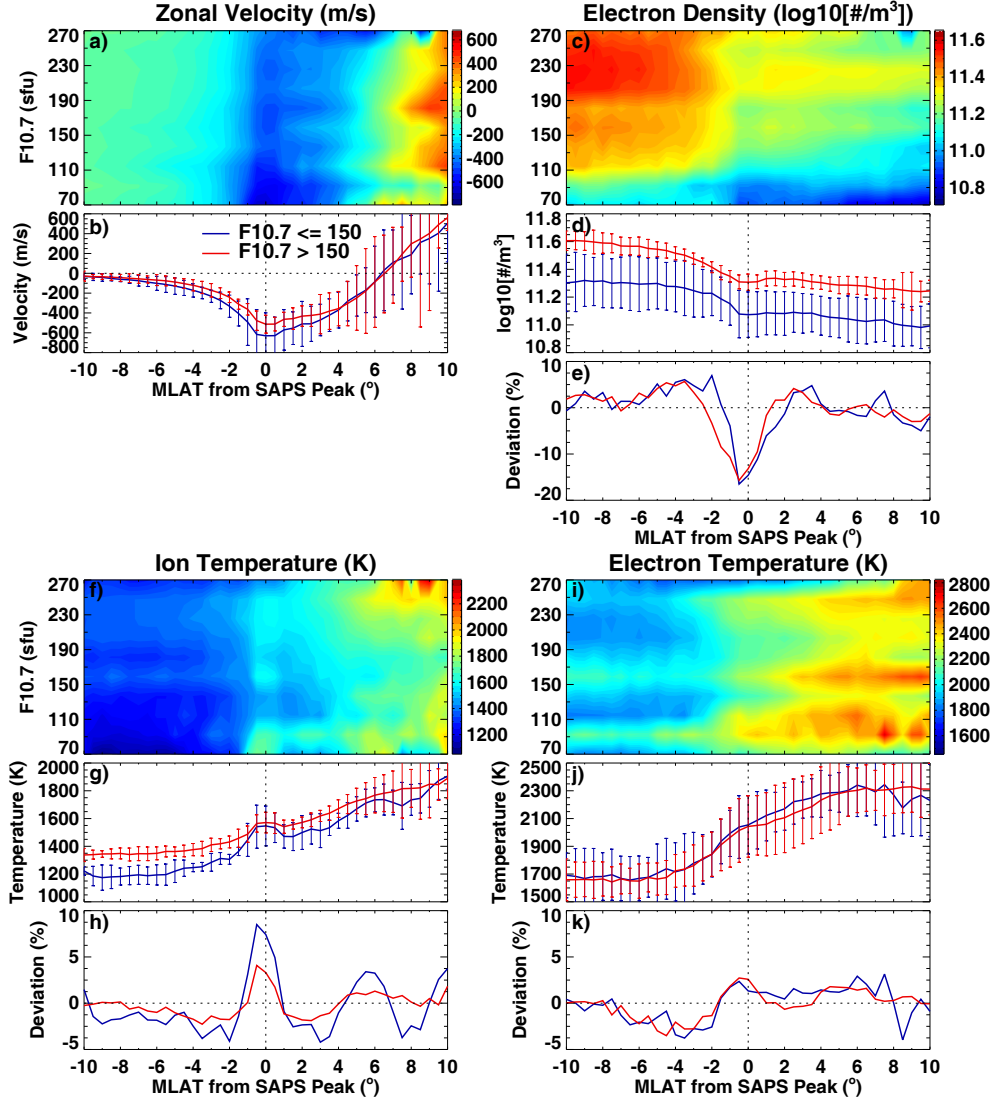
Figure 6. The same as Figure 3, but for different solar activities. The blue lines represent the variation pattern for $F10.7 \leq 150$, while the red lines represent those for $F10.7 > 150$.

the absolute values and the relative enhancements between low and high solar activity periods in our results are approximately the same. This is consistent with observation results from Fok, Kozyra, and Brace (1991) and simulation results from Kozyra et al. (1990), both of which indicated that magnetospheric heat flux and electron densities both vary by an order of magnitude between solar maximum and minimum. For a given level of magnetic activity, the net result is to maintain similar electron temperature enhancements within the solar cycle.

3.5 Interplanetary Magnetic Field Dependence

Figures 7a–7b show the averaged ΔMLAT variation of SAPS-related zonal plasma velocity in 2-D and 1-D formats for different IMF clock angles in the solar wind. It can be seen that both SAPS flow and ion vertical flow are much stronger when the IMF clock angle is between $-180°$ and $-90°$ (i.e., negative By and negative Bz). For IMF Bz dependence, other studies indicate that SAPS will move equatorward with a larger magnitude when IMF Bz becomes stronger southward, a condition often associated with enhanced geomagnetic activity and extended convection pattern (Horvath & Lovell, 2016; Lin et al., 2019). For IMF By dependence, it is known that the main effect of By is to change the shape and orientation of the two-cell convection pattern, in particular when Bz is negative (Heelis, 1984; Heppner & Maynard, 1987; Weimer, 1995). In the Northern Hemisphere, the dusk cell is more crescent-shaped for negative By and more round for positive By, while the dependence of the dawn cell is the reverse (Ruohoniemi & Greenwald, 1996, 2005). Therefore, under the condition of negative By and negative Bz, the sunward returning flow in the vicinity of the whole evening–midnight sector is predominantly westward since it is dominated by the more crescent-shaped dusk cell. This background trend will facilitate SAPS formation and identification through higher westward speed over wider MLT regions, similar to a "downstream acceleration" process. On the contrary, if By is positive, the background convection flow around midnight is predominantly eastward, and the neutral wind flow pattern will also be influenced with a strong eastward zonal wind at subauroral latitudes (McCormac et al., 1985; Thayer et al., 1987). This neutral wind friction tends to prevent sunward plasma flow from gaining high velocity, similar to an "upstream acceleration" process. Thus, our results of the SAPS dependence on IMF are understandable. Moreover, there is a hemispheric asymmetry of By effects on the convection pattern in the Southern Hemisphere (Papitashvili et al., 1994; Leonard et al., 1995), which means that the condition for strong SAPS flow should be more favored with positive By and negative Bz. This point is partially supported by the results given by Karlsson et al. (1998) that the strongest poleward electric fields associated with SAPS are seen exclusively for negative By in the Northern Hemisphere and positive By in the Southern Hemisphere.

Figures 7c–7e show the averaged ΔMLAT variation of SAPS-related electron density for different IMF clock angles in the solar wind. It can be seen that the deepest trough occurs around $\pm180°$ of southward IMF. This is expected, since it is reported that the trough depth will increase with increasing geomagnetic activity due to enhanced dissociative recombination associated with strong frictional heating within SAPS (e.g., Collis & Haggstrom, 1988; Karpachev et al., 1996; Prölss, 2007; Aa et al., 2020). Moreover, the relative deviation of Ne is slightly larger under negative By and negative Bz than other conditions, which is similar to the SAPS distribution reported here. Another point worth noting is that the overall level of electron density is generally lower with positive By and is higher with negative By. One possible explanation is related with the thermosphere wind circulation patterns through collisional interactions with the convecting ions. As mentioned above, the thermosphere wind circulation pattern at mid-to-high latitudes also has an IMF dependence similar to ions: specifically, for positive (negative) By, the size of the dusk (dawn) circulation cell and its neutral wind speed will increase (e.g., McCormac et al., 1985; Thayer et al., 1987; Hernandez et al., 1991; Richmond et al., 2003). Furthermore, around the midnight sector in the Northern Hemisphere, a strong
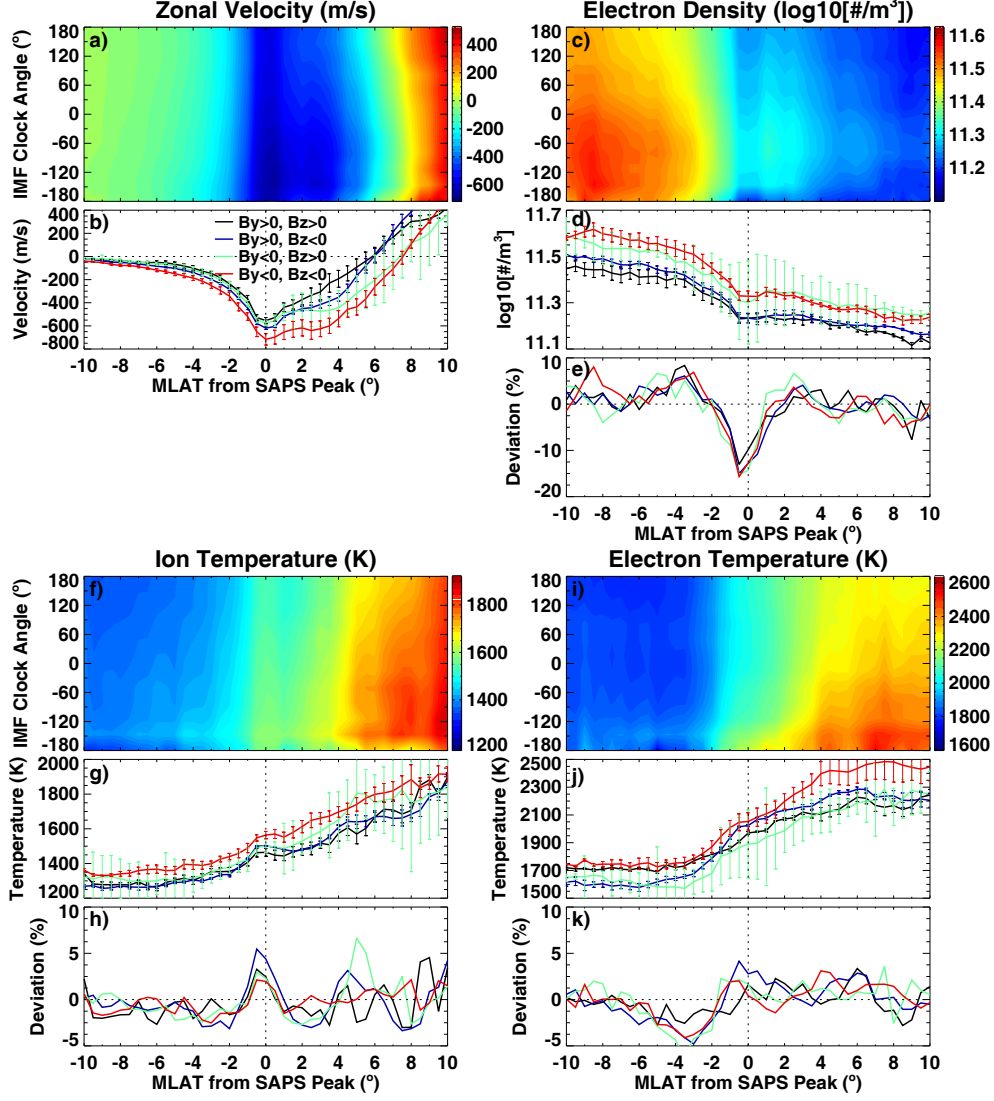
Figure 7. The same as Figure 3, but for different interplanetary magnetic field (IMF) clock angles. In the 1-D plot, four different orientation of IMF By and Bz components are shown by different combinations of colors and line styles.

and positive By will cause stronger eastward zonal wind at high latitudes as well as stronger equatorward winds at lower latitudes due to clockwise diversion driven by Coriolis force, which will amplify the stormtime equatorward surge of thermospheric meridional wind and lead to an equatorward progression of neutral disturbances with reduction of O/N_2 ratio, causing the background electron density to decrease (Rees et al., 1986; Immel et al., 1997; L. Goncharenko et al., 2006; Förster et al., 2008). On the other hand, ion drag is a significant force for modifying neutral winds in the low density region around SAPS (Ferdousi et al., 2019), and enhanced westward neutral wind was found to peak around the same latitude as SAPS flow (H. Wang et al., 2011, 2012). The Coriolis force on the westward wind drives a poleward wind disturbance and can sometimes establish a poleward wind to prevent the storm time equatorward surge (S.-R. Zhang et al., 2015), thus raising the O/N_2 ratio and background electron density. This condition will be more favored with larger SAPS under negative By as mentioned before.

Figures 7f–7h and 7i–7k show the averaged ΔMLAT variation of SAPS-related ion and electron temperature for different IMF clock angles, respectively. Similar to the plasma velocity, both ion and electron temperature have generally larger values when the IMF clock angle is between $-180°$ and $-90°$ though their relative deviation fluctuates between 40–80 K exhibiting no clear IMF dependence. S.-R. Zhang et al. (2016) analyzed the long-term cooling trends of ionospheric ion temperature at Sondrestrom and found that more negative Bz corresponds to Ti reduction in the topside ionosphere during nighttime, possibly due to adiabatic cooling. This may partially inhibit the Ti enhancement effect associated with stronger geomagnetic activity though further study is still needed to quantify the relative contribution of this mechanism.

3.6 Joint heat flow analysis of SAPS region Ne and Te
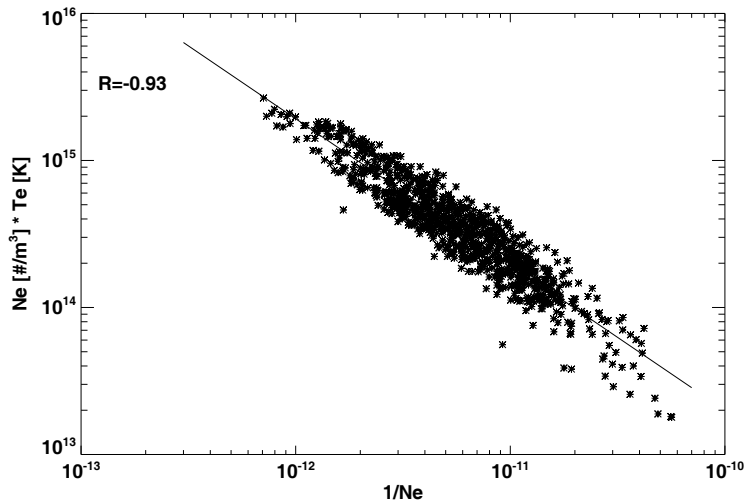
Figure 8. A scatter plot showing the comparion between 1/Ne and Ne×Te around SAPS.

A joint analysis of the combined quantity $Ne\times Te$ is important in understanding the characteristics of heat flow around the SAPS region. It is known that in the F region and topside ionosphere, the thermal electron heating rate is proportional to thermal electron densities, while the dominant electron cooling process is Coulomb collisions with ambient ions, with a cooling rate proportional to Ne^2 (and the difference between

Te and Ti) (Schunk & Nagy, 1978). Thus, many studies have reported negatively correlated Ne and Te relationships under a quasi-steady state of thermal equilibrium (e.g., S.-R. Zhang & Holt, 2004; S.-R. Zhang et al., 2004), with the heat content term of $Ne \times Te$ likely related to $1/Ne$. Figure 8 shows a scatter plot comparison between $Ne \times Te$ and $1/Ne$ from our study with very good correlation (R=-0.93). Results indicate that $Ne \times Te$ is essentially determined by Ne, and Te changes in response to the variation of Ne. This also means that the above-mentioned thermally quasi-steady state is valid for our SAPS data with no large external heating to ionospheric electrons from sources such as soft particle precipitation or field-aligned heat conduction from higher altitudes. Under this assumption, a quantitative relationship between Ne and Te at 300-550 km heights can be approximately derived for SAPS regions from our results as:

$$Te = 10^{\alpha \times log(Ne) + \beta}, \tag{2}$$

where α and β equal to -0.0085 and 3.39, respectively. The uncertainties for these two coefficients are 0.002 and 0.126, respectively. This result is new, and should be further expanded by future coupled ionosphere, plasmasphere, and magnetospheric modeling studies.

4 Conclusions

This paper presents a comprehensive statistical study of the subauroral polarization stream as well as related electron density, ion temperature, and electron temperature by using long-term measurements of Millstone Hill incoherent scatter radar over North American sector during 1979–2019. A superposed epoch analysis technique was used to investigate the distribution patterns of these parameters with respect to MLT, season, geomagnetic activity, solar activity, and IMF orientation, respectively. The statistical results in this study not only confirmed some previously-established characteristics but also proposed new insights on SAPS, such as its solar activity and IMF dependencies.

The main results that further confirmed previously published ones are as follows:

1. SAPS tends to locate at the equatorward boundary of the auroral precipitation with ∼3–4° offset. SAPS has MLT variation with larger magnitude and broader width around dusk than midnight, seasonal asymmetry with higher peak velocity in winter than summer, and geomagnetic dependence with larger velocity during active periods than quiet time.

2. SAPS is usually associated with a midlatitude trough of 15–20% Ne depletion, and the trough depth exhibits an increasing trend with increasing Kp value.

3. The subauroral ion and electron temperature exhibit 3–8% (50–120 K) enhancement associated with SAPS, and both have larger enhancement during geomagnetically active periods. The ion temperature is determined by the altitude-dependent contribution from SAPS-related frictional heating and local heat conduction/advection. The electron temperature is influenced by the thermal interaction between downward heat transfer from ring current and local Coulomb cooling, and lower Ne tends to make the heating (cooling) process more (less) efficient in generating more significant electron temperature enhancement.

The new findings on SAPS features are summarized as follows:

1. The average SAPS detection rate among our database is 5%–15% with two peaks occurring around equinoxes, likely due to enhanced geomagnetic activities during equinoctial periods. SAPS tends to have larger velocity in low solar activity than high solar activity periods, which could be partially attributed to weaker height-integrated Pedersen conductivity around solar minimum.

2. SAPS has a dependence on IMF orientation, which tend to have larger velocity when the IMF clock angle is between $-180°$ and $-90°$ (i.e., negative By and negative Bz). This phenomenon might be collectively interpreted by the Bz-related geomagnetic dependence of SAPS, as well as the By-related dependence of plasma convection and neutral wind patterns.

3. The SAPS-related midlatitude trough has clear MLT and seasonal preference. It has the largest depletion in the postmidnight sector around 00-02 MLT, probably results from extended subauroral plasma stagnation due to the reduced SAPS that is close to the counteracting corotation flow. The trough depth is larger around equinoxes than other seasons, likely due to slightly increased SAPS number and magnitude associated with enhanced geomagnetic activities around equinoxes.

4. The ion and electron temperature enhancement around SAPS peak is generally more pronounced during midnight than dusk. Conditions for ion temperature enhancement are more favored during low solar activity periods, while the electron temperature enhancement is almost constant within solar cycle.

5. SAPS thermal content $Te \times Ne$ is consistent with thermal equilibrium, is strongly dependent on $1/Ne$, and therefore Te exhibits negative correlation with respect to Ne. This result could indicate that external heat input to the ionosphere in SAPS regions through thermal conduction from the plasmasphere is unlikely to be substantial, but this needs to be further explored with future modeling studies.

Acknowledgments

Millstone Hill incoherent scatter radar observation and analysis are part of the US NSF Geospace Facility program under a cooperative agreement AGS-1952737 with Massachusetts Institute of Technology. The same NSF program supports Madrigal Databaset (http://openmadrigal.org) which provides all Millstone Hill radar data used in this work. SRZ and AJC acknowledge the AFOSR support for the MURI Project FA9559-16-1-0364; and AJC, SRZ and LPG acknowledge the ONR Grant N00014-17-1-2186. The F10.7 data is acquired from NASA/GSFC's Space Physics Data Facility's OMNIWeb service (https://cdaweb.gsfc.nasa.gov/). Kp indices are downloaded from Kyoto world data center for Geomagnetism (http://wdc.kugi.kyoto-u.ac.jp/). The DMSP SSJ/4 and SSJ/5 particle detectors were designed and calibrated by Dave Hardy of the Air Force Research Laboratory, and the Auroral Boundary Index (ABI) was downloaded from Madrigal Database (http://cedar.openmadrigal.org), which was also provided by the Air Force Research Laboratory, Kirtland Air Force Base, New Mexico.

References

Aa, E., Zou, S., Erickson, P. J., Zhang, S.-R., & Liu, S. (2020). Statistical analysis of the main ionospheric trough using swarm in situ measurements. *Journal of Geophysical Research: Space Physics*, *125*(3), e2019JA027583. doi: 10.1029/2019JA027583

Afonin, V. V., Bassolo, V. S., Smilauer, J., & Lemaire, J. F. (1997, February). Motion and erosion of the nightside plasmapause region and of the associated subauroral electron temperature enhancement: Cosmos 900 observations. *Journal of Geophysical Research*, *102*(A2), 2093-2104. doi: 10.1029/96JA02497

Anderson, P. C. (2004, Jun). Subauroral electric fields and magnetospheric convection during the April, 2002 geomagnetic storms. *Geophysical Research Letters*, *31*(11), L11801. doi: 10.1029/2004GL019588

Anderson, P. C., Carpenter, D. L., Tsuruda, K., Mukai, T., & Rich, F. J. (2001, Dec). Multisatellite observations of rapid subauroral ion drifts (SAID). *Journal of Geophysical Research: Space Physics*, *106*(A12), 29585-29600. doi: 10.1029/2001JA000128

Anderson, P. C., Hanson, W. B., Heelis, R. A., Craven, J. D., Baker, D. N., & Frank, L. A. (1993, Apr). A proposed production model of rapid subauroral ion drifts and their relationship to substorm evolution. *Journal of Geophysical Research*, *98*(A4), 6069-6078. doi: 10.1029/92JA01975

Anderson, P. C., Heelis, R. A., & Hanson, W. B. (1991, Apr). The ionospheric signatures of rapid subauroral ion drifts. *Journal of Geophysical Research*, *96*(A4), 5785-5792. doi: 10.1029/90JA02651

Buonsanto, M. J., Foster, J. C., & Sipler, D. P. (1992, Feb). Observations From Millstone Hill During the Geomagnetic Disturbances of March and April 1990. *Journal of Geophysical Research*, *97*(A2), 1225-1243. doi: 10.1029/91JA02428

Califf, S., Li, X., Wolf, R. A., Zhao, H., Jaynes, A. N., Wilder, F. D., ... Redmon, R. (2016, Jun). Large-amplitude electric fields in the inner magnetosphere: Van Allen Probes observations of subauroral polarization streams. *Journal of Geophysical Research: Space Physics*, *121*(6), 5294-5306. doi: 10.1002/2015JA022252

Carbary, J. F. (2005, Oct). A Kp-based model of auroral boundaries. *Space Weather*, *3*(10), S10001. doi: 10.1029/2005SW000162

Clausen, L. B. N., Baker, J. B. H., Ruohoniemi, J. M., Greenwald, R. A., Thomas, E. G., Shepherd, S. G., ... Sazykin, S. (2012, May). Large-scale observations of a subauroral polarization stream by midlatitude SuperDARN radars: Instantaneous longitudinal velocity variations. *Journal of Geophysical Research*, *117*(A5), A05306. doi: 10.1029/2011JA017232

Collis, P. N., & Haggstrom, I. (1988). Plasma convection and auroral precipitation processes associated with the main ionospheric trough at high latitudes. *Journal of Atmospheric and Terrestrial Physics*, *50*, 389-404. doi: 10.1016/0021-9169(88)90024-4

De Keyser, J. (1999, Jun). Formation and evolution of subauroral ion drifts in the course of a substorm. *Journal of Geophysical Research*, *104*(A6), 12339-12350. doi: 10.1029/1999JA900109

Ebihara, Y., Nishitani, N., Kikuchi, T., Ogawa, T., Hosokawa, K., Fok, M. C., & Thomsen, M. F. (2009, Jan). Dynamical property of storm time subauroral rapid flows as a manifestation of complex structures of the plasma pressure in the inner magnetosphere. *Journal of Geophysical Research*, *114*(A1), A01306. doi: 10.1029/2008JA013614

Erickson, P. J., Beroz, F., & Miskin, M. Z. (2011, Mar). Statistical characterization of the American sector subauroral polarization stream using incoherent scatter radar. *Journal of Geophysical Research: Space Physics*, *116*, A00J21. doi: 10.1029/2010JA015738

Erickson, P. J., Foster, J. C., & Holt, J. M. (2002, April). Inferred electric field variability in the polarization jet from Millstone Hill E region coherent scatter observations. *Radio Science*, *37*(2), 1027. doi: 10.1029/2000RS002531

Erickson, P. J., Goncharenko, L. P., Nicolls, M. J., Ruohoniemi, M., & Kelley, M. C. (2010, March). Dynamics of North American sector ionospheric and thermospheric response during the November 2004 superstorm. *Journal of Atmospheric and Solar-Terrestrial Physics*, *72*(4), 292-301. doi: 10.1016/j.jastp.2009.04.001

Erickson, P. J., Matsui, H., Foster, J. C., Torbert, R. B., Ergun, R. E., Khotyaintsev, Y. V., ... Magnes, W. (2016, Jul). Multipoint MMS observations of fine-scale SAPS structure in the inner magnetosphere. *Geophysical Research Letters*, *43*(14), 7294-7300. doi: 10.1002/2016GL069174

Evans, J. V. (1970, January). Midlatitude ionospheric temperatures during three magnetic storms in 1965. *Journal of Geophysical Research*, *75*(25), 4803. doi: 10.1029/JA075i025p04803

Evans, J. V. (1973, January). Seasonal and sunspot cycle variations of F Region electron temperatures and protonospheric heat fluxes. *Journal of Geophysical Research*, *78*(13), 2344. doi: 10.1029/JA078i013p02344

Ferdousi, B., Nishimura, Y., Maruyama, N., & Lyons, L. R. (2019, March). Subauroral Neutral Wind Driving and Its Feedback to SAPS During the 17 March 2013 Geomagnetic Storm. *Journal of Geophysical Research: Space Physics*, *124*(3), 2323-2337. doi: 10.1029/2018JA026193

Fok, M. C., Kozyra, J. U., & Brace, L. H. (1991, February). Solar cycle variation in the subauroral electron temperature enhancement: Comparison of AE-C and DE 2 satellite observations. *Journal of Geophysical Research*, *96*(A2), 1861-1866. doi: 10.1029/90JA02377

Fok, M. C., Kozyra, J. U., Warren, M. F., & Brace, L. H. (1991, June). Seasonal variations in the subauroral electron temperature enhancement. *Journal of Geophysical Research*, *96*(A6), 9773-9780. doi: 10.1029/91JA00791

Förster, M., Rentz, S., Köhler, W., Liu, H., & Haaland, S. E. (2008, June). IMF dependence of high-latitude thermospheric wind pattern derived from CHAMP cross-track measurements. *Annales Geophysicae*, *26*(6), 1581-1595. doi: 10.5194/angeo-26-1581-2008

Foster, J. C. (1993, February). Storm time plasma transport at middle and high latitudes. *Journal of Geophysical Research*, *98*(A2), 1675-1690. doi: 10.1029/92JA02032

Foster, J. C., & Burke, W. J. (2002). SAPS: A new categorization for sub-auroral electric fields. *EOS Transactions*, *83*(36), 393. doi: 10.1029/2002EO000289

Foster, J. C., Coster, A. J., Erickson, P. J., Holt, J. M., Lind, F. D., Rideout, W.,

... Rich, F. J. (2005, Sep).   Multiradar observations of the polar tongue of ionization. *Journal of Geophysical Research (Space Physics)*, *110*(A9), A09S31. doi: 10.1029/2004JA010928

Foster, J. C., Erickson, P. J., Coster, A. J., Thaller, S., Tao, J., Wygant, J. R., & Bonnell, J. W. (2014, February). Storm time observations of plasmasphere erosion flux in the magnetosphere and ionosphere. *Geophysical Research Letters*, *41*(3), 762-768. doi: 10.1002/2013GL059124

Foster, J. C., Rideout, W., Sandel, B., Forrester, W. T., & Rich, F. J.   (2007, Mar).   On the relationship of SAPS to storm-enhanced density.   *Journal of Atmospheric and Solar-Terrestrial Physics*, *69*(3), 303-313.   doi: 10.1016/j.jastp.2006.07.021

Foster, J. C., & Vo, H. B.   (2002, Dec).   Average characteristics and activity dependence of the subauroral polarization stream.   *Journal of Geophysical Research: Space Physics*, *107*(A12), 1475. doi: 10.1029/2002JA009409

Galperin, Y., Ponomarov, Y., & Zosinova, A.   (1974).   Plasma convection in polar ionosphere. *Annales de Geophysique*, *30*(1-7).

Gkioulidou, M., Wang, C.-P., Lyons, L. R., & Wolf, R. A.   (2009, July).   Formation of the Harang reversal and its dependence on plasma sheet conditions: Rice convection model simulations. *Journal of Geophysical Research :Space Physics*, *114*(A7), A07204. doi: 10.1029/2008JA013955

Goldstein, J., Burch, J. L., Sandel, B. R., Mende, S. B., Brandt, P. C., & Hairston, M. R.   (2005, Mar).   Coupled response of the inner magnetosphere and ionosphere on 17 April 2002.   *Journal of Geophysical Research*, *110*(A3), A03205. doi: 10.1029/2004JA010712

Goldstein, J., Sandel, B. R., Thomsen, M. F., Spasojević, M., & Reiff, P. H.   (2004, Mar).   Simultaneous remote sensing and in situ observations of plasmaspheric drainage plumes.   *Journal of Geophysical Research*, *109*(A3), A03202. doi: 10 .1029/2003JA010281

Goncharenko, L., Salah, J., Crowley, G., Paxton, L. J., Zhang, Y., Coster, A., . . . Taran, V.   (2006, March).   Large variations in the thermosphere and ionosphere during minor geomagnetic disturbances in April 2002 and their association with IMF B$_y$. *Journal of Geophysical Research*, *111*(A3), A03303.   doi: 10.1029/2004JA010683

Goncharenko, L. P., Foster, J. C., Coster, A. J., Huang, C., Aponte, N., & Paxton, L. J.   (2007, Jul).   Observations of a positive storm phase on September 10, 2005.   *Journal of Atmospheric and Solar-Terrestrial Physics*, *69*(10-11), 1253-1272. doi: 10.1016/j.jastp.2006.09.011

Gussenhoven, M. S., Hardy, D. A., & Burke, W. J. (1981, Feb). DMSP/F2 electron observations of equatorward auroral boundaries and their relationship to magnetospheric electric fields.   *Journal of Geophysical Research*, *86*(A2), 768-778. doi: 10.1029/JA086iA02p00768

Gussenhoven, M. S., Hardy, D. A., & Heinemann, N.   (1983, Jul).   Systematics of the equatorward diffuse auroral boundary.   *Journal of Geophysical Research*, *88*(A7), 5692-5708. doi: 10.1029/JA088iA07p05692

Gussenhoven, M. S., Hardy, D. A., & Heinemann, N.   (1987, Apr).   The equatorward boundary of auroral ion precipitation.   *Journal of Geophysical Research*, *92*(A4), 3273-3283. doi: 10.1029/JA092iA04p03273

Hardy, D. A., Gussenhoven, M. S., & Brautigam, D. (1989, Jan). A statistical model of auroral ion precipitation. *Journal of Geophysical Research*, *94*(A1), 370-392. doi: 10.1029/JA094iA01p00370

Hardy, D. A., Gussenhoven, M. S., Raistrick, R., & McNeil, W. J.   (1987, November). Statistical and functional representations of the pattern of auroral energy flux, number flux, and conductivity. *Journal of Geophysical Research*, *92*(A11), 12275-12294. doi: 10.1029/JA092iA11p12275

Hardy, D. A., Holeman, E. G., Burke, W. J., Gentile, L. C., & Bounar, K. H. (2008,

Jun). Probability distributions of electron precipitation at high magnetic latitudes. *Journal of Geophysical Research*, *113*(A6), A06305. doi: 10.1029/2007JA012746

He, F., Zhang, X., & Chen, B. (2014, Jun). Solar cycle, seasonal, and diurnal variations of subauroral ion drifts: Statistical results. *Journal of Geophysical Research: Space Physics*, *119*(6), 5076-5086. doi: 10.1002/2014JA019807

He, F., Zhang, X., Wang, W., Liu, L., Ren, Z., Yue, X., ... Wang, H. (2018, Apr). Large-Scale Structure of Subauroral Polarization Streams During the Main Phase of a Severe Geomagnetic Storm. *Journal of Geophysical Research: Space Physics*, *123*(4), 2964-2973. doi: 10.1002/2018JA025234

He, F., Zhang, X., Wang, W., & Wan, W. (2017, Nov). Different Evolution Patterns of Subauroral Polarization Streams (SAPS) During Intense Storms and Quiet Time Substorms. *Geophysical Research Letters*, *44*(21), 10,796-10,804. doi: 10.1002/2017GL075449

Heelis, R. A. (1984, May). The effects of interplanetary magnetic field orientation on dayside high-latitude ionospheric convection. *Journal of Geophysical Research*, *89*(A5), 2873-2880. doi: 10.1029/JA089iA05p02873

Heelis, R. A., Bailey, G. J., Sellek, R., Moffett, R. J., & Jenkins, B. (1993, December). Field-aligned drifts in subauroral ion drift events. *Journal of Geophysical Research*, *98*(A12), 21493-21500. doi: 10.1029/93JA02209

Heinemann, N. C., Gussenhoven, M. S., Hardy, D. A., Rich, F. J., & Yeh, H. C. (1989, Oct). Electron/ion precipitation differences in relation to region 2 field-aligned currents. *Journal of Geophysical Research*, *94*(A10), 13593-13600. doi: 10.1029/JA094iA10p13593

Heppner, J. P., & Maynard, N. C. (1987, May). Empirical high-latitude electric field models. *Journal of Geophysical Research*, *92*(A5), 4467-4490. doi: 10.1029/JA092iA05p04467

Hernandez, G., McCormac, F. G., & Smith, R. W. (1991, April). Austral thermospheric wind circulation and interplanetary magnetic field orientation. *Journal of Geophysical Research*, *96*(A4), 5777-5783. doi: 10.1029/90JA02458

Horvath, I., & Lovell, B. C. (2016, Feb). Structured subauroral polarization streams and related auroral undulations occurring on the storm day of 21 January 2005. *Journal of Geophysical Research: Space Physics*, *121*(2), 1680-1695. doi: 10.1002/2015JA022057

Huang, C.-S., & Foster, J. C. (2007, Nov). Correlation of the subauroral polarization streams (SAPS) with the Dst index during severe magnetic storms. *Journal of Geophysical Research: Space Physics*, *112*(A11), A11302. doi: 10.1029/2007JA012584

Immel, T. J., Craven, J. D., & Frank, L. A. (1997, April). Influence of IMF B_y on large-scale decreases of O column density at middle latitudes. *Journal of Atmospheric and Solar-Terrestrial Physics*, *59*, 725-737. doi: 10.1016/S1364-6826(96)00099-5

Karlsson, T., Marklund, G. T., Blomberg, L. G., & Mälkki, A. (1998, Mar). Subauroral electric fields observed by the Freja satellite: A statistical study. *Journal of Geophysical Research*, *103*(A3), 4327-4342. doi: 10.1029/97JA00333

Karpachev, A. T. (2003). The dependence of the main ionospheric trough shape on longitude, altitude, season, local time, and solar and magnetic activity. *Geomagnetism and Aeronomy*, *43*(2), 239-251.

Karpachev, A. T. (2019). Variations in the Winter Troughs' Position With Local Time, Longitude, and Solar Activity in the Northern and Southern Hemispheres. *Journal of Geophysical Research: Space Physics*, *124*(10), 8039-8055. doi: 10.1029/2019JA026631

Karpachev, A. T., Deminov, M. G., & Afonin, V. V. (1996, Jan). Model of the mid-latitude ionospheric trough on the base of Cosmos-900 and Intercosmos-19 satellites data. *Advances in Space Research*, *18*(6), 221-230. doi:

10.1016/0273-1177(95)00928-0

Kelley, M. C., Vlasov, M. N., Foster, J. C., & Coster, A. J.   (2004, October).   A quantitative explanation for the phenomenon known as storm-enhanced density. *Geophysical Research Letters*, *31*(19), L19809.   doi: 10.1029/2004GL020875

Koustov, A. V., Drayton, R. A., Makarevich, R. A., McWilliams, K. A., St-Maurice, J. P., Kikuchi, T., & Frey, H. U.   (2006, Jul).   Observations of high-velocity SAPS-like flows with the King Salmon SuperDARN radar. *Annales Geophysicae*, *24*(6), 1591-1608. doi: 10.5194/angeo-24-1591-2006

Kozyra, J. U., Brace, L. H., Cravens, T. E., & Nagy, A. F.   (1986, October).   A statistical study of the subauroral electron temperature enhancement using Dynamics Explorer-2 Langmuir probe observations. *Journal of Geophysical Research*, *91*(A10), 11270-11280. doi: 10.1029/JA091iA10p11270

Kozyra, J. U., Valladares, C. E., Carlson, H. C., Buonsanto, M. J., & Slater, D. W.   (1990, August).   A theoretical study of the seasonal and solar cycle variations of stable Auroa Red arcs. *Journal of Geophysical Research*, *95*(A8), 12219-12234. doi: 10.1029/JA095iA08p12219

Kunduri, B. S. R., Baker, J. B. H., Ruohoniemi, J. M., Clausen, L. B. N., Grocott, A., Thomas, E. G., ... Talaat, E. R.   (2012, Aug).   An examination of inter-hemispheric conjugacy in a subauroral polarization stream. *Journal of Geophysical Research*, *117*(A8), A08225. doi: 10.1029/2012JA017784

Kunduri, B. S. R., Baker, J. B. H., Ruohoniemi, J. M., Nishitani, N., Oksavik, K., Erickson, P. J., ... Miller, E. S.   (2018, Sep).   A New Empirical Model of the Subauroral Polarization Stream. *Journal of Geophysical Research: Space Physics*, *123*(9), 7342-7357. doi: 10.1029/2018JA025690

Kunduri, B. S. R., Baker, J. B. H., Ruohoniemi, J. M., Thomas, E. G., Shepherd, S. G., & Sterne, K. T.   (2017, Jun).   Statistical characterization of the large-scale structure of the subauroral polarization stream. *Journal of Geophysical Research: Space Physics*, *122*(6), 6035-6048. doi: 10.1002/2017JA024131

Landry, R. G., & Anderson, P. C.   (2018, Apr).   An Auroral Boundary-Oriented Model of Subauroral Polarization Streams (SAPS). *Journal of Geophysical Research: Space Physics*, *123*(4), 3154-3169. doi: 10.1002/2017JA024921

Le, H., Yang, N., Liu, L., Chen, Y., & Zhang, H.   (2017).   The latitudinal structure of nighttime ionospheric TEC and its empirical orthogonal functions model over North American sector. *Journal of Geophysical Research: Space Physics*, *122*(1), 963-977. doi: 10.1002/2016JA023361

Lejosne, S., & Mozer, F. S.   (2017, Sep).   Subauroral Polarization Streams (SAPS) Duration as Determined From Van Allen Probe Successive Electric Drift Measurements. *Geophysical Research Letters*, *44*(18), 9134-9141.   doi: 10.1002/2017GL074985

Leonard, J. M., Pinnock, M., Rodger, A. S., Dudeney, J. R., Greenwald, R. A., & Baker, K. B.   (1995, July).   Ionospheric plasma convection in the southern hemisphere. *Journal of Atmospheric and Terrestrial Physics*, *57*, 889-897. doi: 10.1016/0021-9169(94)00070-5

Lin, D., Wang, W., Scales, W. A., Pham, K., Liu, J., Zhang, B., ... Maimaiti, M.   (2019, Jul). SAPS in the 17 March 2013 Storm Event: Initial Results From the Coupled Magnetosphere-Ionosphere-Thermosphere Model. *Journal of Geophysical Research: Space Physics*, *124*(7), 6212-6225. doi: 10.1029/2019JA026698

Lyatsky, W., Newell, P. T., & Hamza, A. (2001, Jan). Solar illumination as cause of the equinoctial preference for geomagnetic activity. *Geophysical Research Letters*, *28*(12), 2353-2356. doi: 10.1029/2000GL012803

Makarevich, R. A., Kellerman, A. C., Bogdanova, Y. V., & Koustov, A. V.   (2009, Apr).   Time evolution of the subauroral electric fields: A case study during a sequence of two substorms. *Journal of Geophysical Research*, *114*(A4), A04312. doi: 10.1029/2008JA013944

McCormac, F. G., Killeen, T. L., Gombosi, E., Hays, P. B., & Spencer, N. W. (1985, April). Configuration of the high-latitude thermosphere neutral circulation for IMF B$_y$ negative and positive. *Geophysical Research Letters*, *12*(4), 155-158. doi: 10.1029/GL012i004p00155

Mendillo, M. (2006, December). Storms in the ionosphere: Patterns and processes for total electron content. *Reviews of Geophysics*, *44*(4), RG4001. doi: 10.1029/2005RG000193

Mishin, E. V. (2013, Sep). Interaction of substorm injections with the subauroral geospace: 1. Multispacecraft observations of SAID. *Journal of Geophysical Research: Space Physics*, *118*(9), 5782-5796. doi: 10.1002/jgra.50548

Mishin, E. V. (2016, Jul). SAPS onset timing during substorms and the westward traveling surge. *Geophysical Research Letters*, *43*(13), 6687-6693. doi: 10.1002/2016GL069693

Mishin, E. V., Nishimura, Y., & Foster, J. (2017, Aug). SAPS/SAID revisited: A causal relation to the substorm current wedge. *Journal of Geophysical Research: Space Physics*, *122*(8), 8516-8535. doi: 10.1002/2017JA024263

Mishin, E. V., Puhl-Quinn, P. A., & Santolik, O. (2010, Apr). SAID: A turbulent plasmaspheric boundary layer. *Geophysical Research Letters*, *37*(7), L07106. doi: 10.1029/2010GL042929

Moffett, R. J., Ennis, A. E., Bailey, G. J., Heelis, R. A., & Brace, L. H. (1998, April). Electron temperatures during rapid subauroral ion drift events. *Annales Geophysicae*, *16*(4), 450-459. doi: 10.1007/s00585-998-0450-x

Moffett, R. J., & Quegan, S. (1983). The mid-latitude trough in the electron concentration of the ionospheric F-layer - A review of observations and modelling. *Journal of Atmospheric and Terrestrial Physics*, *45*, 315-343. doi: 10.1016/S0021-9169(83)80038-5

Muldrew, D. B. (1965). F-Layer Ionization Troughs Deduced from Alouette Data. *Journal of Geophysical Research*, *70*(11), 2635-2650. doi: 10.1029/JZ070i011p02635

Nagano, H., Nishitani, N., & Hori, T. (2015, Aug). Occurrence characteristics and lowest speed limit of subauroral polarization stream (SAPS) observed by the SuperDARN Hokkaido East radar. *Earth, Planets, and Space*, *67*, 126. doi: 10.1186/s40623-015-0299-7

Oksavik, K., Greenwald, R. A., Ruohoniemi, J. M., Hairston, M. R., Paxton, L. J., Baker, J. B. H., ... Barnes, R. J. (2006, Jun). First observations of the temporal/spatial variation of the sub-auroral polarization stream from the SuperDARN Wallops HF radar. *Geophysical Research Letters*, *33*(12), L12104. doi: 10.1029/2006GL026256

Papitashvili, V. O., Belov, B. A., Faermark, D. S., Feldstein, Y. I., Golyshev, S. A., Gromova, L. I., & Levitin, A. E. (1994, July). Electric potential patterns in the northern and southern polar regions parameterized by the interplanetary magnetic field. *Journal of Geophysical Research*, *99*(A7), 13251-13262. doi: 10.1029/94JA00822

Parkinson, M. L., Pinnock, M., Wild, J. A., Lester, M., Yeoman, T. K., Milan, S. E., ... Kikuchi, T. (2005, Jun). Interhemispheric asymmetries in the occurrence of magnetically conjugate sub-auroral polarisation streams. *Annales Geophysicae*, *23*(4), 1371-1390. doi: 10.5194/angeo-23-1371-2005

Pintér, B., Thom, S. D., Balthazor, R., Vo, H., & Bailey, G. J. (2006, Oct). Modeling subauroral polarization streams equatorward of the plasmapause footprints. *Journal of Geophysical Research*, *111*(A10), A10306. doi: 10.1029/2005JA011457

Prölss, G. W. (2006, August). Subauroral electron temperature enhancement in the nighttime ionosphere. *Annales Geophysicae*, *24*(7), 1871-1885. doi: 10.5194/angeo-24-1871-2006

Prölss, G. W. (2007, Mar). The equatorward wall of the subauroral trough in the af-

ternoon/evening sector. *Annales Geophysicae*, *25*(3), 645-659. doi: 10.5194/angeo-25-645-2007

Raeder, J., Cramer, W. D., Jensen, J., Fuller-Rowell, T., Maruyama, N., Toffoletto, F., & Vo, H. (2016, Nov). Sub-Auroral Polarization Streams: A complex interaction between the magnetosphere, ionosphere, and thermosphere. In *Journal of physics conference series* (Vol. 767, p. 012021). doi: 10.1088/1742-6596/767/1/012021

Rees, D., Fuller-Rowell, T. J., Gordon, R., Smith, M. F., Maynard, N. C., Heppner, J. P., . . . Killeen, T. L. (1986, January). A theoretical and empirical study of the response of the high latitude thermosphere to the sense of the "Y" component of the interplanetary magnetic field. *Planet. Space Sci.*, *34*(1), 1-40. doi: 10.1016/0032-0633(86)90100-5

Rich, F. J., & Hairston, M. (1994, March). Large-scale convection patterns observed by DMSP. *Journal of Geophysical Research*, *99*(A3), 3827-3844. doi: 10.1029/93JA03296

Richards, P. G., & Torr, D. G. (1986, August). Thermal coupling of conjugate ionospheres and the tilt of the earth's magnetic field. *Journal of Geophysical Research*, *91*(A8), 9017-9022. doi: 10.1029/JA091iA08p09017

Richmond, A. D., LathuillèRe, C., & Vennerstroem, S. (2003, February). Winds in the high-latitude lower thermosphere: Dependence on the interplanetary magnetic field. *Journal of Geophysical Research*, *108*(A2), 1066. doi: 10.1029/2002JA009493

Robinson, R. M., & Vondrak, R. R. (1984, June). Measurements of E region ionization and conductivity produced by solar illumination at high latitudes. *Journal of Geophysical Research*, *89*(A6), 3951-3956. doi: 10.1029/JA089iA06p03951

Rodger, A. S. (2008, Jan). The mid-latitude trough—Revisited. *Washington DC American Geophysical Union Geophysical Monograph Series*, *181*, 25-33. doi: 10.1029/181GM04

Ruohoniemi, J. M., & Greenwald, R. A. (1996, October). Statistical patterns of high-latitude convection obtained from Goose Bay HF radar observations. *Journal of Geophysical Research*, *101*(A10), 21743-21764. doi: 10.1029/96JA01584

Ruohoniemi, J. M., & Greenwald, R. A. (2005, September). Dependencies of high-latitude plasma convection: Consideration of interplanetary magnetic field, seasonal, and universal time factors in statistical patterns. *Journal of Geophysical Research*, *110*(A9), A09204. doi: 10.1029/2004JA010815

Russell, C. T., & McPherron, R. L. (1973, Jan). Semiannual variation of geomagnetic activity. *Journal of Geophysical Research*, *78*(1), 92. doi: 10.1029/JA078i001p00092

Schunk, R. W., Banks, P. M., & Raitt, W. J. (1976). Effects of electric fields and other processes upon the nighttime high-latitude F layer. *Journal of Geophysical Research*, *81*(19), 3271. doi: 10.1029/JA081i019p03271

Schunk, R. W., & Nagy, A. F. (1978, August). Electron temperatures in the F region of the ionosphere: theory and observation. *Reviews of Geophysics and Space Physics*, *16*, 355-399. doi: 10.1029/RG016i003p00355

Schunk, R. W., & Nagy, A. F. (2000). *Ionospheres: physics, plasma physics, and chemistry.* Cambridge University Press.

Spiro, R. W., Heelis, R. A., & Hanson, W. B. (1978, September). Ion convection and the formation of the mid-latitude F region ionization trough. *Journal of Geophysical Research*, *83*(A9), 4255-4264. doi: 10.1029/JA083iA09p04255

Spiro, R. W., Heelis, R. A., & Hanson, W. B. (1979, Aug). Rapid subauroral ion drifts observed by Atmosphere Explorer C. *Geophysical Research Letters*, *6*(8), 657-660. doi: 10.1029/GL006i008p00657

Thayer, J. P., Killeen, T. L., McCormac, F. G., Tschan, C. R., Ponthieu, J. J., & Spencer, N. W. (1987, December). Thermospheric neutral wind signatures

dependent on the east-west component of the interplanetary magnetic field for Northern and Southern Hemispheres as measured from Dynamics Explorer-2. *Annales Geophysicae*, *5*, 363-368.

Tulunay, Y. K., & Sayers, J. (1971, Nov). Characteristics of the mid-latitude trough as determined by the electron density experiment on Ariel III. *Journal of Atmospheric and Terrestrial Physics*, *33*(11), 1737-1761. doi: 10.1016/0021-9169(71)90221-2

Voiculescu, M., & Nygrén, T. (2007). IMF effect on ionospheric trough occurrence at equinoxes. *Advances in Space Research*, *40*(12), 1935-1940. doi: 10.1016/j.asr .2007.04.108

Wang, H., & Lühr, H. (2013, Sep). Seasonal variation of the ion upflow in the topside ionosphere during SAPS (subauroral polarization stream) periods. *Annales Geophysicae*, *31*(9), 1521-1534. doi: 10.5194/angeo-31-1521-2013

Wang, H., Lühr, H., Häusler, K., & Ritter, P. (2011, Mar). Effect of subauroral polarization streams on the thermosphere: A statistical study. *Journal of Geophysical Research*, *116*(A3), A03312. doi: 10.1029/2010JA016236

Wang, H., Lühr, H., & Ma, S. (2012, Apr). The relation between subauroral polarization streams, westward ion fluxes, and zonal wind: Seasonal and hemispheric variations. *Journal of Geophysical Research*, *117*(A4), A04323. doi: 10.1029/2011JA017378

Wang, H., Ridley, A. J., Lühr, H., Liemohn, M. W., & Ma, S. Y. (2008, Dec). Statistical study of the subauroral polarization stream: Its dependence on the cross-polar cap potential and subauroral conductance. *Journal of Geophysical Research: Space Physics*, *113*(A12), A12311. doi: 10.1029/2008JA013529

Wang, W., Burns, A. G., & Killeen, T. L. (2006, November). A numerical study of the response of ionospheric electron temperature to geomagnetic activity. *Journal of Geophysical Research*, *111*(A11), A11301. doi: 10.1029/2006JA011698

Wang, W., Talaat, E. R., Burns, A., Emery, B., Hsieh, S., Lei, J., & Xu, J. (2012, Jul). Thermosphere and ionosphere response to subauroral polarization streams (SAPS): Model simulations. *Journal of Geophysical Research*, *117*(A7), A07301. doi: 10.1029/2012JA017656

Wang, Z., Zou, S., Shepherd, S. G., Liang, J., Gjerloev, J. W., Ruohoniemi, J. M., ... Wygant, J. R. (2019, March). Multi-instrument Observations of Mesoscale Enhancement of Subauroral Polarization Stream Associated With an Injection. *Journal of Geophysical Research: Space Physics*, *124*(3), 1770-1784. doi: 10.1029/2019JA026535

Watanabe, S., Oyama, K.-I., & Abe, T. (1989, November). Electron temperature structure around mid latitude ionospheric trough. *Planet. Space Sci.*, *37*(11), 1453-1460. doi: 10.1016/0032-0633(89)90115-3

Weimer, D. R. (1995, October). Models of high-latitude electric potentials derived with a least error fit of spherical harmonic coefficients. *Journal of Geophysical Research*, *100*(A10), 19595-19608. doi: 10.1029/95JA01755

Werner, S., & Prölss, G. W. (1997). The position of the ionospheric trough as a function of local time and magnetic activity. *Advances in Space Research*, *20*(9), 1717-1722. doi: 10.1016/S0273-1177(97)00578-4

Yeh, H. C., & Foster, J. C. (1990, June). Storm time heavy ion outflow at mid-latitude. *Journal of Geophysical Research*, *95*(A6), 7881-7891. doi: 10.1029/JA095iA06p07881

Yeh, H. C., Foster, J. C., Rich, F. J., & Swider, W. (1991, Apr). Storm time electric field penetration observed at mid-latitude. *Journal of Geophysical Research*, *96*(A4), 5707-5721. doi: 10.1029/90JA02751

Yu, Y., Jordanova, V., Zou, S., Heelis, R., Ruohoniemi, M., & Wygant, J. (2015, Mar). Modeling subauroral polarization streams during the 17 March 2013 storm. *Journal of Geophysical Research: Space Physics*, *120*(3), 1738-1750. doi: 10.1002/2014JA020371

Yuan, Z., Xiong, Y., Qiao, Z., Li, H., Huang, S., Wang, D., ... Wang, J.   (2016, Feb).   A subauroral polarization stream driven by field-aligned currents associated with precipitating energetic ions caused by EMIC waves: A case study. *Journal of Geophysical Research: Space Physics*, *121*(2), 1696-1705.   doi: 10.1002/2015JA021804

Zhang, Q., Liu, Y., Zhang, Q.-H., Xing, Z., Wang, Y., & Ma, Y.   (2020, Mar).   Statistical study of ion upflow associated with subauroral polarization streams (SAPS) at substorm time.   *Journal of Geophysical Research: Space Physics*, *125*(7), e2019JA027163. doi: 10.1029/2019JA027163

Zhang, S.-R., Erickson, P. J., Foster, J. C., Holt, J. M., Coster, A. J., Makela, J. J., ... Kerr, R. B.   (2015, July).   Thermospheric poleward wind surge at midlatitudes during great storm intervals.   *Geophysical Research Letters*, *42*(13), 5132-5140. doi: 10.1002/2015GL064836

Zhang, S.-R., Erickson, P. J., Zhang, Y., Wang, W., Huang, C., Coster, A. J., ... Kerr, R.   (2017, Jan).   Observations of ion-neutral coupling associated with strong electrodynamic disturbances during the 2015 St. Patrick's Day storm. *Journal of Geophysical Research: Space Physics*, *122*(1), 1314-1337.   doi: 10.1002/2016JA023307

Zhang, S.-R., & Holt, J. M.   (2004, January).   Ionospheric plasma temperatures during 1976-2001 over Millstone Hill. *Advances in Space Research*, *33*(6), 963-969. doi: 10.1016/j.asr.2003.07.012

Zhang, S.-R., & Holt, J. M.   (2007, Jun).   Ionospheric climatology and variability from long-term and multiple incoherent scatter radar observations: Climatology in eastern American sector.   *Journal of Geophysical Research*, *112*(A6), A06328. doi: 10.1029/2006JA012206

Zhang, S.-R., Holt, J. M., Erickson, P. J., Goncharenko, L. P., Nicolls, M. J., McCready, M., & Kelly, J.   (2016, September).   Ionospheric ion temperature climate and upper atmospheric long-term cooling.   *Journal of Geophysical Research: Space Physics*, *121*(9), 8951-8968. doi: 10.1002/2016JA022971

Zhang, S.-R., Holt, J. M., Zalucha, A. M., & Amory-Mazaudier, C.   (2004, November).   Midlatitude ionospheric plasma temperature climatology and empirical model based on Saint Santin incoherent scatter radar data from 1966 to 1987.   *Journal of Geophysical Research: Space Physics*, *109*(A11), A11311.   doi: 10.1029/2004JA010709

Zhang, X., He, F., Wang, W., & Chen, B.   (2015, Jun).   Hemispheric asymmetry of subauroral ion drifts: Statistical results.   *Journal of Geophysical Research: Space Physics*, *120*(6), 4544-4554. doi: 10.1002/2015JA021016

Zheng, Y., Brandt, P. C., Lui, A. T. Y., & Fok, M.-C.   (2008, Apr).   On ionospheric trough conductance and subauroral polarization streams: Simulation results.   *Journal of Geophysical Research*, *113*(A4), A04209.   doi: 10.1029/2007JA012532

Zou, S., Lyons, L. R., Nicolls, M. J., Heinselman, C. J., & Mende, S. B.   (2009, December).   Nightside ionospheric electrodynamics associated with substorms: PFISR and THEMIS ASI observations.   *Journal of Geophysical Research: Space Physics*, *114*(A12), A12301. doi: 10.1029/2009JA014259

Zou, S., Lyons, L. R., Wang, C. P., Boudouridis, A., Ruohoniemi, J. M., Anderson, P. C., ... Devlin, J. C.   (2009).   On the coupling between the Harang reversal evolution and substorm dynamics: A synthesis of SuperDARN, DMSP, and IMAGE observations.   *Journal of Geophysical Research: Space Physics*, *114*(A1), A01205. doi: 10.1029/2008JA013449

Zou, S., Moldwin, M. B., Ridley, A. J., Nicolls, M. J., Coster, A. J., Thomas, E. G., & Ruohoniemi, J. M.   (2014, Oct).   On the generation/decay of the storm-enhanced density plumes: Role of the convection flow and field-aligned ion flow. *Journal of Geophysical Research: Space Physics*, *119*(10), 8543-8559. doi: 10.1002/2014JA020408

1153   Zou, S., Ridley, A. J., Moldwin, M. B., Nicolls, M. J., Coster, A. J., Thomas, E. G.,
1154   & Ruohoniemi, J. M. (2013, December). Multi-instrument observations of SED
1155   during 24-25 October 2011 storm: Implications for SED formation processes.
1156   *Journal of Geophysical Research (Space Physics)*, *118*(12), 7798-7809.   doi:
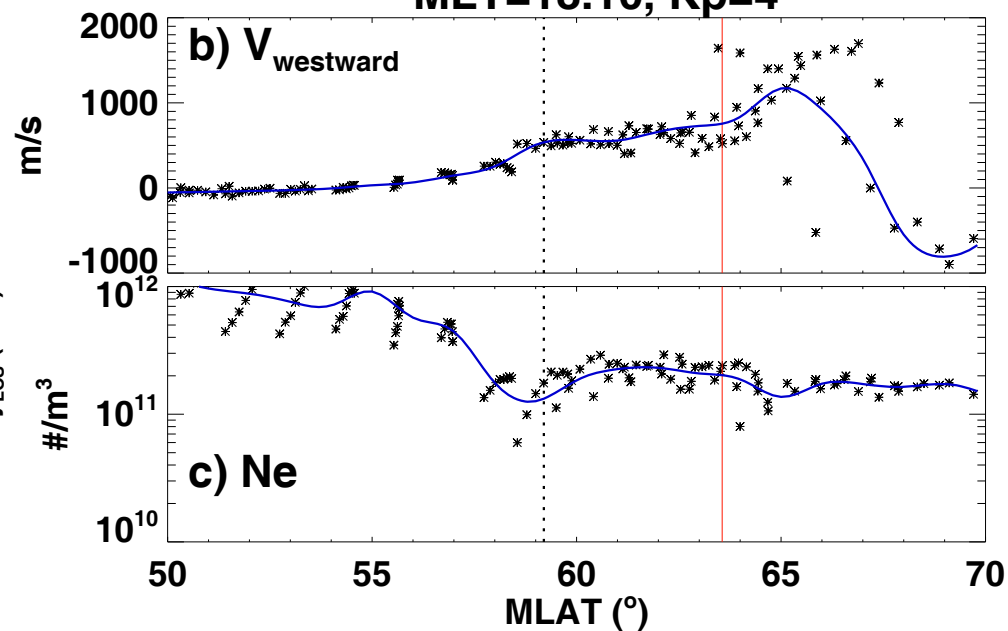1157   10.1002/2013JA018860

Figure 1.

a) ISR Scan @ 10-MAR-1989 00:39 UT

Velocity$_{LOS}$ (m/s)

MLT=18.10, Kp=4

b) V$_{westward}$

m/s

c) Ne

#/m^3

MLAT (^{o})
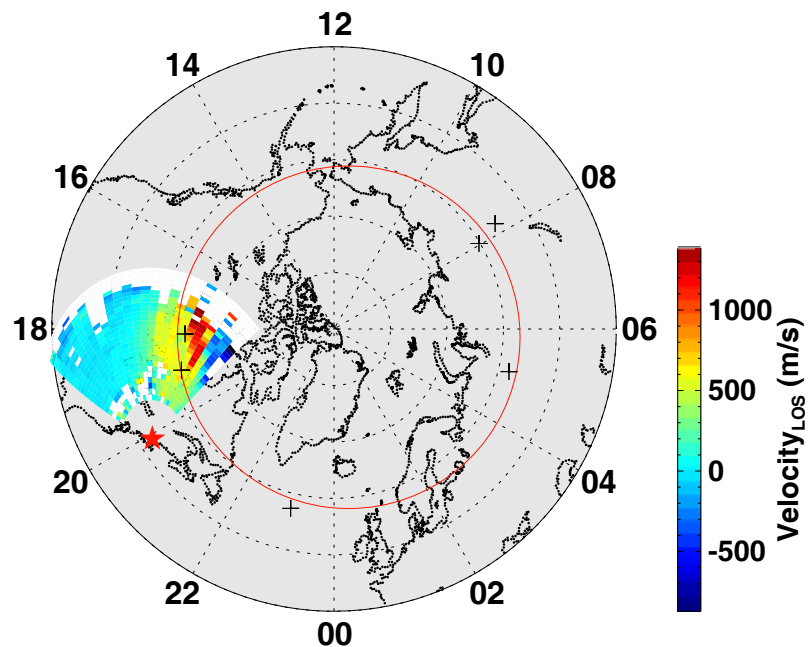
d) ISR Scan @ 09-MAR-1989 07:24 UT

Velocity$_{LOS}$ (m/s)

MLT= 0.93, Kp=3

e) V$_{westward}$

m/s

f) Ne

#/m^3

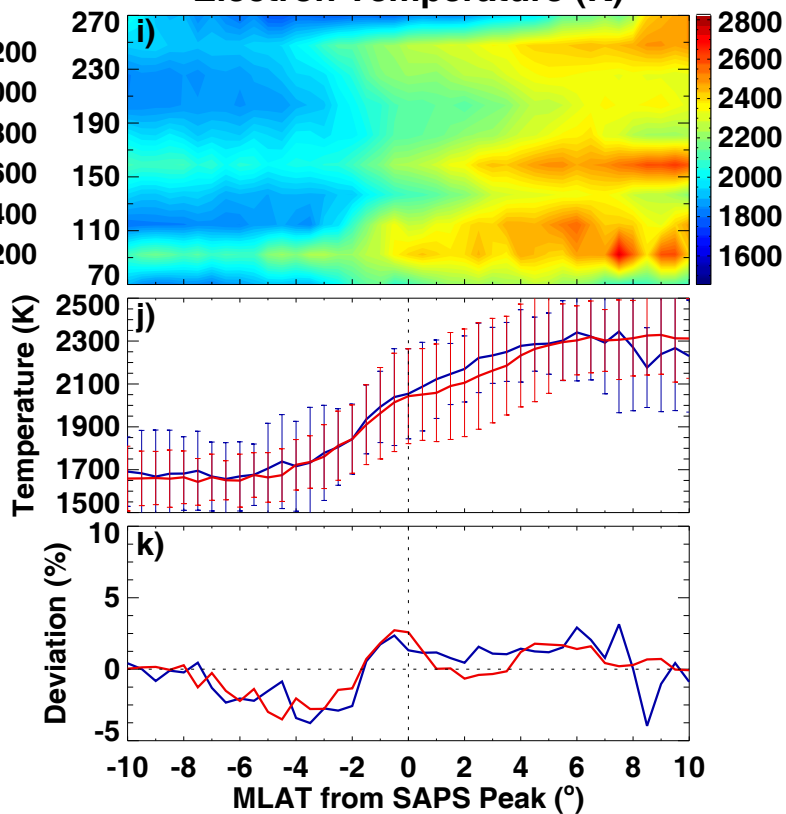MLAT (^{o})
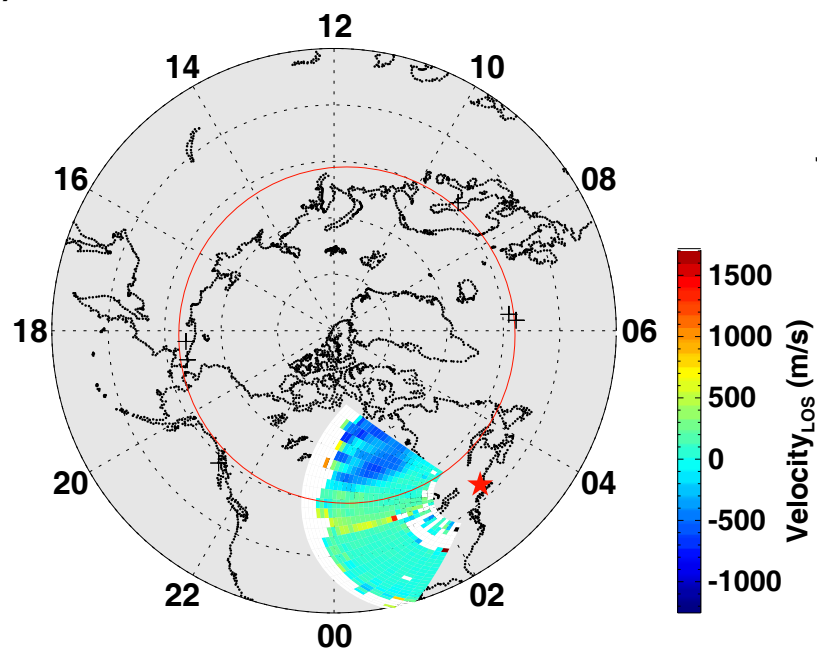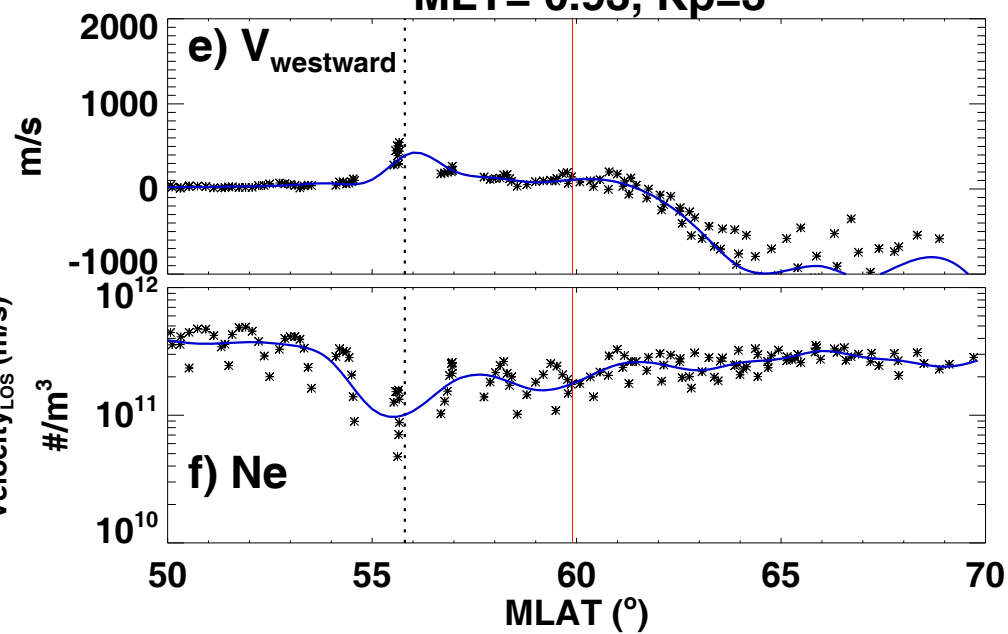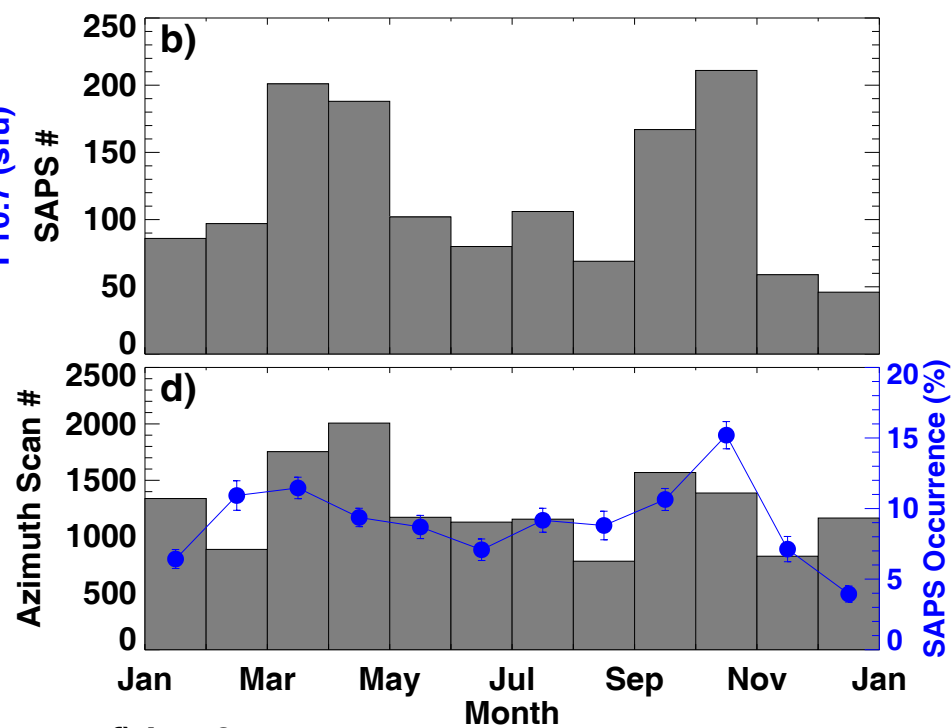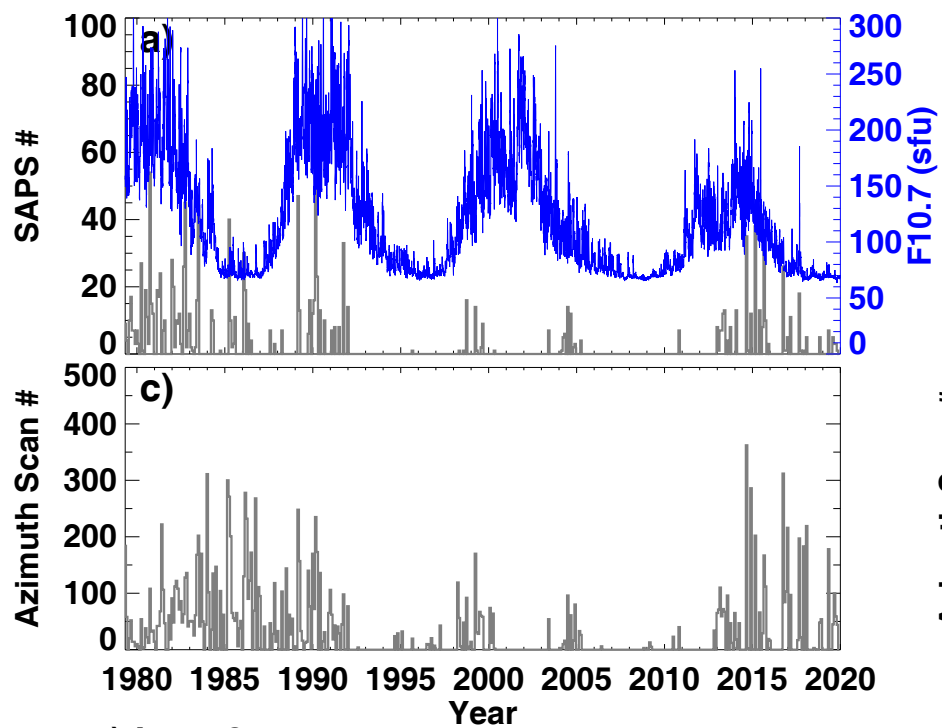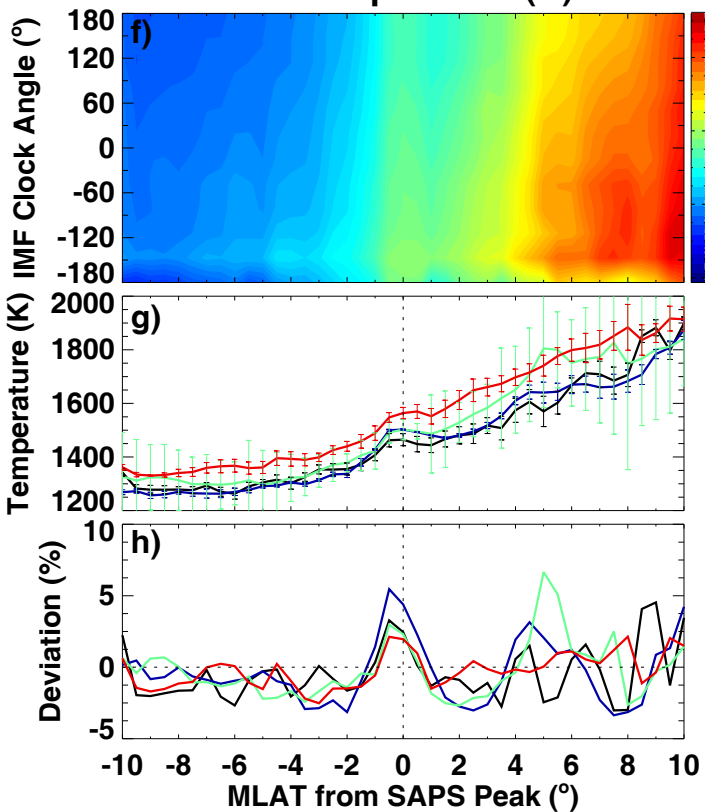
Figure 2.
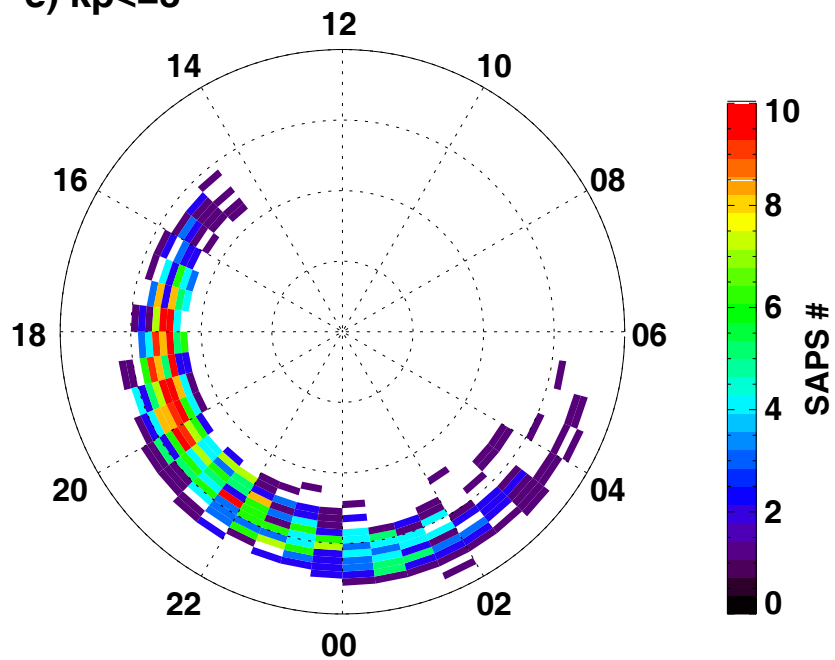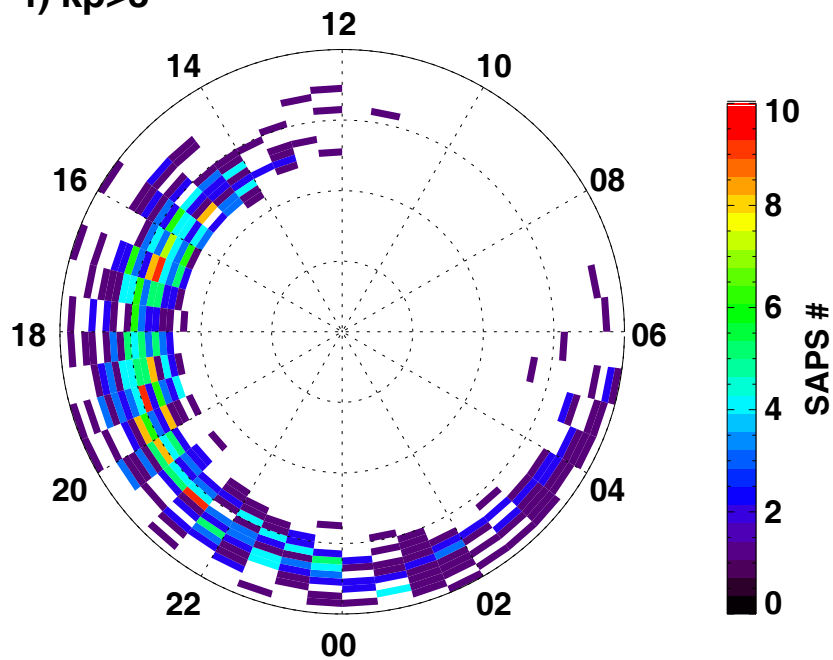
Figure 3.

Figure 4.

Figure 5.

Zonal Velocity (m/s)
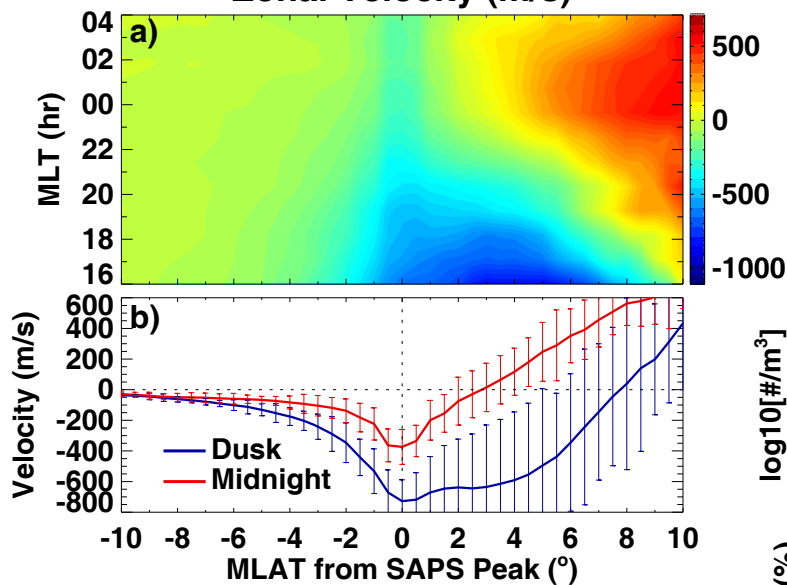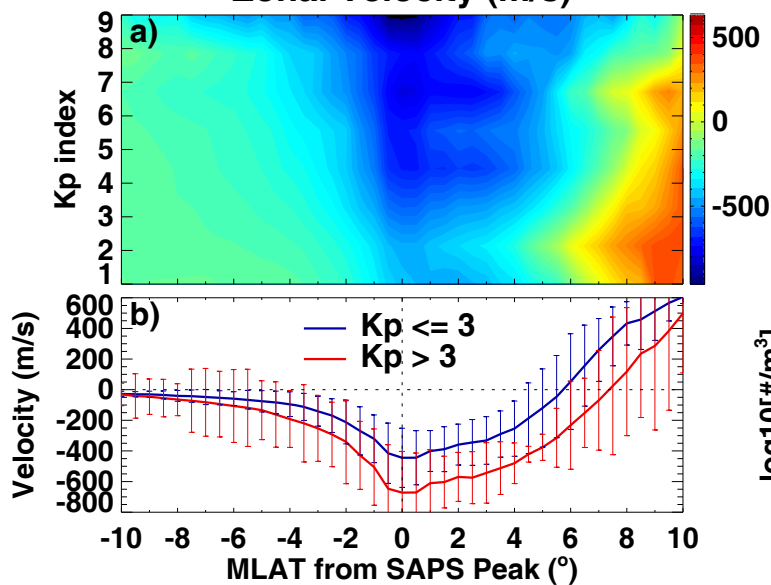
Electron Density (log10[#/m³])
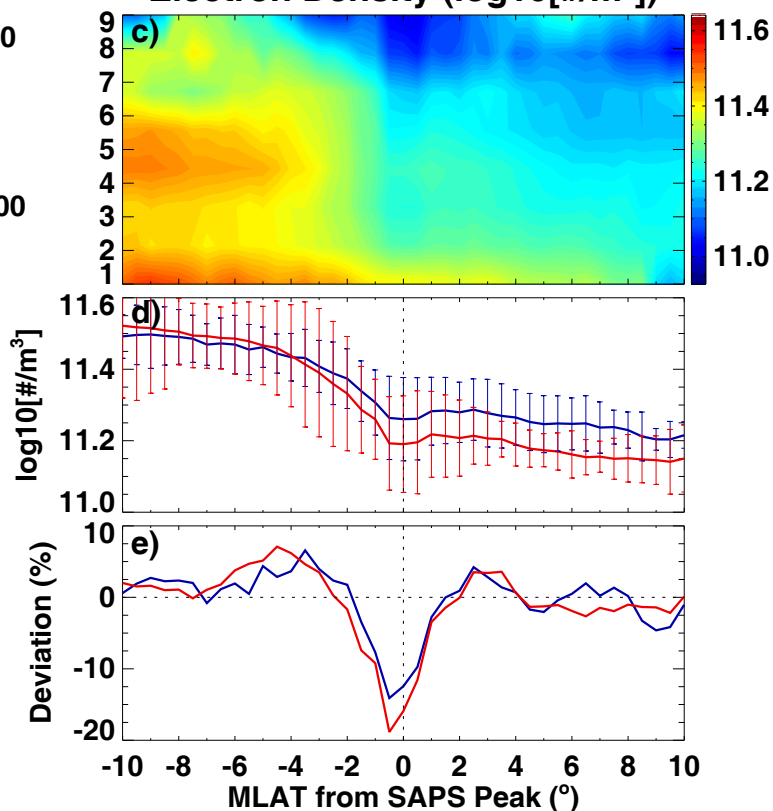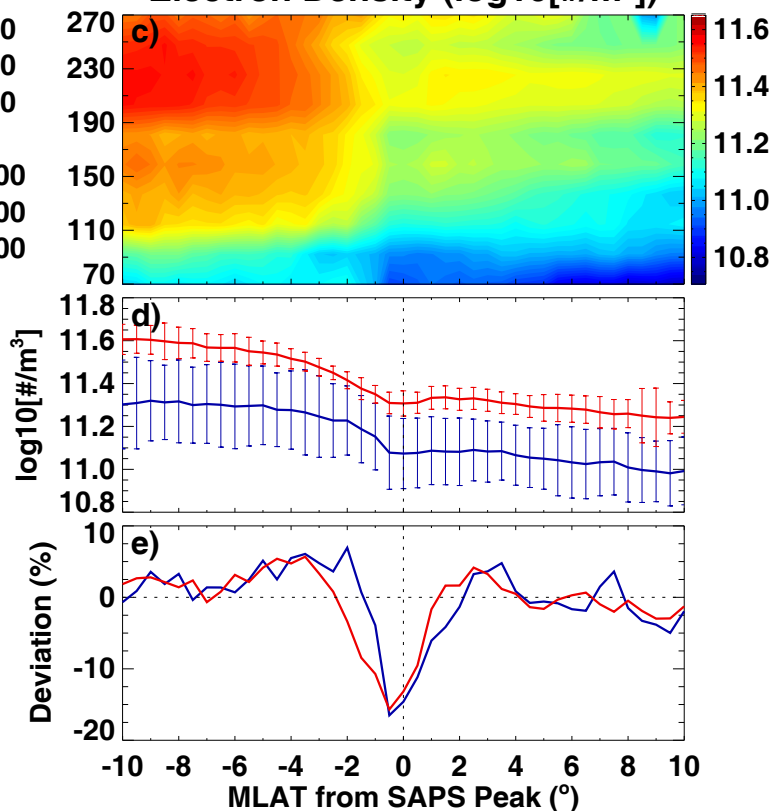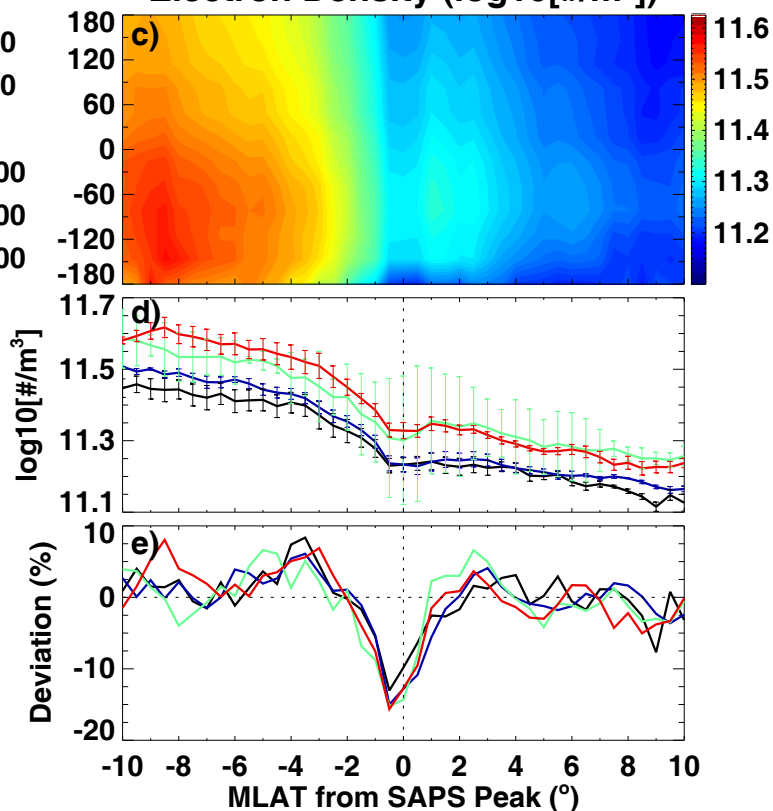
Ion Temperature (K)

Electron Temperature (K)

Figure 6.

Figure 7.

Zonal Velocity (m/s)

a)

b)

- By>0, Bz>0 (black)
- By>0, Bz<0 (blue)
- By<0, Bz>0 (green)
- By<0, Bz<0 (red)

Electron Density (log10[#/m³])

c)

d)

e)

Ion Temperature (K)

f)

g)

h)

Electron Temperature (K)

i)

j)

k)

Figure 8.